Research Article:

Title: *ONC201 in combination with paxalisib is a therapeutic strategy for diffuse midline glioma*

Authors:

Evangeline R. Jackson[1,2,#], Ryan J. Duchatel[1,2,#], Dilana E. Staudt[1,2,#], Mika L. Persson[1,2], Abdul Mannan[1,2], Sridevi Yadavilli[3,4], Sarah Parackal[5,6], Shaye Game[5,6], Wai Chin Chong[5,6], W. Samantha N. Jayasekara [5,6], Marion Le Grand[7], Padraic S. Kearney[1,2], Alicia M. Douglas[1,2], Izac J. Findlay[1,2], Zacary P. Germon[1,2], Holly P. McEwen[1,2], Tyrone S. Beitaki[1,2], Adjanie Patabendige[8,9], David A. Skerrett-Byrne[10,11], Brett Nixon[10,11], Nathan D. Smith[12], Bryan Day[13], Neevika Manoharan[14], Sumanth Nagabushan[14], Jordan R. Hansford[15], Dinisha Govender[16], Geoff B. McCowage[16], Ron Firestein[5,6], Meegan Howlett[17], Raelene Endersby[17], Nicholas G. Gottardo[17,18], Frank Alvaro[2,19], Sebastian M. Waszak[20,21], Martin R. Larsen[22], Yolanda Colino-Sanguino[23,24], Fatima Valdes-Mora[23,24], Andria Rakotomalala[25,26], Samuel Meignan[25,26], Eddy Pasquier[7,27], Nicolas André[7,27,28], Esther Hulleman[29], David D. Eisenstat[30,31], Nicholas A. Vitanza[32,33], Javad Nazarian[3,34,35], Carl Koschmann[36], Sabine Mueller[34,37], Jason E. Cain[5,6], Matthew D. Dun[1,2,38,39]

Affiliations:

[1] Cancer Signalling Research Group, School of Biomedical Sciences and Pharmacy, College of Health, Medicine and Wellbeing, University of Newcastle, Callaghan, NSW, AUSTRALIA.

[2] Precision Medicine Research Program, Hunter Medical Research Institute, New Lambton Heights, NSW, AUSTRALIA.

[3] Center for Genetic Medicine Research, Children's National Hospital, Washington, DC, USA.

[4] Brain Tumor Institute, Children's National Hospital, Washington, DC, USA.

[5] Centre for Cancer Research, Hudson Institute of Medical Research, Clayton, VIC, AUSTRALIA.

[6] Department of Molecular and Translational Science, Monash University, Clayton, VIC, AUSTRALIA.

[7] Centre de Recherche en Cancérologie de Marseille, Aix-Marseille Université, Inserm, CNRS, Institut Paoli Calmettes, Marseille, FRANCE.

[8] Brain Barriers Group, School of Biomedical Sciences and Pharmacy, College of Health, Medicine and Wellbeing, University of Newcastle, University Drive, Callaghan, NSW, AUSTRALIA.

[9] Department of Biology, Edge Hill University, Ormskirk, UK.

[10] School of Environmental and Life Sciences, College of Engineering, Science and Environment, University of Newcastle, Callaghan, NSW, AUSTRALIA.

[11] Infertility and Reproduction Research Program, Hunter Medical Research Institute, New Lambton Heights, NSW, AUSTRALIA.

[12] Analytical and Biomolecular Research Facility Advanced Mass Spectrometry Unit, University of Newcastle, Callaghan, NSW, AUSTRALIA.

[13] QIMR Berghofer Medical Research Institute, Herston, QLD, AUSTRALIA.

[14] Department of Paediatric Oncology, Sydney Children's Hospital, Randwick, NSW, AUSTRALIA

[15] Michael Rice Cancer Centre, Women's and Children's Hospital, South Australia Health and Medical Research Institute, South Australia ImmunoGenomics Cancer Institute, University of Adelaide, Adelaide, SA, AUSTRALIA.

[16] Department of Oncology, The Children's Hospital at Westmead, Westmead, NSW, AUSTRALIA.

[17] Brain Tumor Research Program, Telethon Kids Cancer Centre, Telethon Kids Institute, University of Western Australia, Perth, WA, AUSTRALIA.

[18] Department of Pediatric and Adolescent Oncology and Hematology, Perth Children's Hospital, Perth, WA, AUSTRALIA.

[19] John Hunter Children's Hospital, New Lambton Heights, NSW, AUSTRALIA.

[20] Centre for Molecular Medicine Norway (NCMM), Nordic EMBL Partnership, University of Oslo and Oslo University Hospital, Oslo, NORWAY.

[21] Department of Neurology, University of California, San Francisco, San Francisco, CA, USA.

[22] Department of Biochemistry and Molecular Biology, University of Southern Denmark, Odense M, DENMARK.

[23] Cancer Epigenetics Biology and Therapeutics, Precision Medicine Theme, Children's Cancer Institute, Sydney, NSW, AUSTRALIA

[24] School of Women's and Children's Health, University of NSW, Sydney, NSW, AUSTRALIA

[25] Tumorigenesis and Resistance to Treatment Unit, Centre Oscar Lambret, Lille, FRANCE

[26] University of Lille, CNRS, Inserm, CHU Lille, UMR9020-U1277, CANTHER, Cancer Heterogeneity Plasticity and Resistance to Therapies, Lille, FRANCE

[27] Metronomics Global Health Initiative, Marseille, FRANCE.

[28] Department of Pediatric Oncology, La Timone Children's Hospital, AP-HM, Marseille, FRANCE

[29] Princess Máxima Center for Pediatric Oncology, Utrecht, THE NETHERLANDS.

[30] Children's Cancer Centre, The Royal Children's Hospital Melbourne, Parkville, Victoria, AUSTRALIA

[31] Neuro-Oncology Laboratory, Murdoch Children's Research Institute, Department of Paediatrics, University of Melbourne, Parkville, Victoria, AUSTRALIA

[32] Ben Towne Center for Childhood Cancer Research, Seattle Children's Research Institute, Seattle, WA, USA

[33] Division of Pediatric Hematology/Oncology, Department of Pediatrics, Seattle Children's Hospital, Seattle, WA, USA

[34] Department of Pediatrics, University Children's Hospital Zurich, Zurich, SWITZERLAND.

[35] The George Washington University, School of Medicine and Health Sciences, Washington, DC, USA.

[36] Division of Pediatric Hematology/Oncology, Department of Pediatrics, University of Michigan, Ann Arbor, MI, USA.

[37] Department of Neurology, Neurosurgery and Pediatric, University of California, San Francisco, CA, USA.

[38] Paediatric Program, Mark Hughes Foundation Centre for Brain Cancer Research, College of Health, Medicine, and Wellbeing, Callaghan, NSW, AUSTRALIA

[39] Lead contact

[#] These authors shared the first authorship for this work.

Additional information:

Funding:

Funding group:

- Award group:
  - Funder(s): NHMRC Investigator Grant.
  - Award Id(s): GNT1173892.
- Award group:
  - Funder(s): Chad Tough Defeat DIPG
- Award group:
  - Funder(s): Tiwari Foundation
- Award group:
  - Funder(s): DIPG/DMG Collaborative

Corresponding authors:

Matthew D. Dun Ph.D.

University Drive, Callaghan, NSW 2308, Australia

Phone: +61 2 4921 5693

Email: matt.dun@newcastle.edu.au, Twitter: @MattDun17

Sabine Mueller M.D., Ph.D., MAS.

Department of Neurology, Neurosurgery and Pediatrics, University of California, San Francisco, 675 Nelson Lane Ring, Room 402, San Francisco, CA 94158. U.S.A.

Phone: +1 415 476 3831

E-mail: sabine.mueller@ucsf.edu

Jason E. Cain Ph.D.

27–31 Wright Street, Clayton, VIC 3168, Australia

Phone: +61 3 8572 2720

Email: jason.cain@hudson.org.au

Carl Koschmann M.D.

3520D MSRB 1, 1150 W Medical Center Dr., Ann Arbor MI, 48109

Phone: +1 734 936 9814

Email: ckoschma@med.umich.edu

Javad Nazarian Ph.D.

Department of Oncology, Children's Research Center, University Children's Hospital

Zürich, Balgrist Campus, Lengghalde 5, 8008 Zürich, Switzerland

Phone: +41 44 266 3776

Email: Javad.Nazarian@kispi.uzh.ch

Conflict of interest:

M.D. Dun is a director of the not-for-profit charity RUN DIPG Ltd.

Word count: 5983

Figures 6, **Supplementary Figures** 11, and **Supplementary Tables** 10.

Abstract

Diffuse midline gliomas (DMG), including diffuse intrinsic pontine gliomas (DIPGs), are the most lethal of childhood cancers. Palliative radiotherapy is the only established treatment, with median patient survival of 9-11 months. ONC201 is a DRD2 antagonist and ClpP agonist that has shown preclinical and emerging clinical efficacy in DMG. However, further work is needed to identify the mechanisms of response of DIPGs to ONC201 treatment and to determine whether recurring genomic features influence response. Using a systems-biological approach, we showed that ONC201 elicits potent agonism of the mitochondrial protease ClpP to drive proteolysis of electron transport chain and tricarboxylic acid cycle proteins. DIPGs harboring *PIK3CA*-mutations showed increased sensitivity to ONC201, while those harboring *TP53*-mutations were more resistant. Metabolic adaptation and reduced sensitivity to ONC201 was promoted by redox-activated PI3K/Akt signaling, which could be counteracted using the brain penetrant PI3K/Akt inhibitor, paxalisib. Together, these discoveries coupled with the powerful anti-DIPG/DMG pharmacokinetic and pharmacodynamic properties of ONC201 and paxalisib have provided the rationale for the ongoing DIPG/DMG phase II combination clinical trial NCT05009992.

50-word statement of significance

PI3K/Akt signaling promotes metabolic adaptation to ONC201-mediated disruption of mitochondrial energy homeostasis in diffuse intrinsic pontine glioma, highlighting the utility of a combination treatment strategy employing ONC201 and the PI3K/Akt inhibitor paxalisib.

Introduction

High-grade gliomas (HGGs) are responsible for 10-15% of all pediatric central nervous system (CNS) cancers, but account for over 40% of deaths (1). Diffuse midline gliomas (DMG), including those of the brainstem (diffuse intrinsic pontine glioma - DIPG) are universally fatal childhood malignancies and responsible for half of all pediatric HGG diagnoses (2). Despite half a century of clinical trials, radiotherapy (RT) remains the only life prolonging treatment for DIPG, with the median overall survival (OS) remaining stagnant at 9-11 months post-diagnosis, and <10% of patients with pontine tumors surviving more than two years post-diagnosis (3,4). The diffuse and infiltrative growth characteristics of DIPG which enmesh the critical structures of the brainstem make surgical resection extremely challenging. However, over the last 10 years image-guided stereotactic biopsy at diagnosis has been shown to be safe and feasible (5), helping to isolate tumor tissue to identify the recurring molecular (6) and immunological (7) features of the disease.

Global loss of trimethylation at lysine 27 (K27) of histone H3 drives epigenetic dysregulation in primitive neuronal stem cells/oligodendrocyte precursor cells, caused by a methionine to lysine substitution (H3K27M) in either *HIST1H3B* (H3.1) or *H3F3A* (H3.3) genes (8-10) or through the overexpression of *EZHIP* (EZH inhibitory protein) in patients harboring wildtype H3 (11). These H3-alterations inhibit the catalysis of H3K27 trimethylation by the polycomb repressive complex 2 (PRC2) (12) and co-occur with mutations in tumor suppressor and signaling genes (13). Together, these changes promote the activity of oncogenic signaling cascades that sustain mitogenesis, immune system avoidance and drive cellular immortality (14).

Preliminary clinical efficacy for the oral, small molecule imipridone anticancer therapy, ONC201, has been reported in patients diagnosed with DIPG (15) and recurrent H3K27M DMG (16). Previous studies in hematological (17), colorectal (18), breast (19), uterine (20), and non-midline brain cancers (such as glioblastoma) (21), showed ONC201 triggered p53-independent cancer cell apoptosis driven in part by an atypical integrated stress response, initiating expression of the anti-tumor protein TRAIL (tumor necrosis factor-related apoptosis-inducing ligand) (22,23). The identification of a durable objective response observed in a patient with a secondary glioblastoma harboring a H3.3K27M mutation encouraged continued testing in patients with these mutations, such as DIPG (21).

Described as a dopamine receptor D2 (DRD2) selective antagonist, corroborated by Bayesian machine-learning approaches (24), more recent studies show ONC201 is also a potent agonist of the ATP-dependent Clp protease proteolytic subunit (ClpP), a mitochondrial protein that degrades mitochondrial respiratory chain proteins to disrupt energy homeostasis (23,25). Recently, mRNA expression analysis correlated *CLPP* expression with tumor grade and overall survival in DMG (25). These studies also demonstrated that DMG cell lines with sensitivity to ONC201 and ONC206 (a

fluorinated analog of ONC201 in a phase I pediatric clinical trial for DMG PNOC023, NCT04732065), impaired tumor cell metabolism and caused mitochondrial damage, inducing reactive oxygen species (ROS) production to activate an integrative stress response and apoptosis *in vitro* and *in vivo.*

Metabolic effects highlight the potential of ONC201 for the treatment of DIPG, potentially circumventing the inter- and intra-tumoral heterogeneity that has previously plagued the use of precision-therapy based approaches (6). Indeed, ONC201 induces a state of energy depletion as outlined by a significant decrease in ATP levels and a hypo-phosphorylated state in glioblastoma (26). Potentially, ONC201 represents an important first step in the establishment of a recognized targeted treatment strategy for some patients with H3K27-altered DMG; however, monotherapeutic benefits are transient, whilst for other patients ONC201 offers no survival improvements and these individuals succumb quickly (27).

Here we employ a systems-wide approach to identify combination strategies to increase the therapeutic response to ONC201, thereby providing the preclinical and preliminary clinical evidence for the commencement of the phase II clinical trial to test ONC201 in combination with the potent brain-penetrant PI3K/Akt inhibitor, paxalisib (28,29), for the treatment of H3K27M DIPG and DMG patients at diagnosis and disease progression (NCT05009992).

Materials and Methods

Reagents

Unless otherwise stated, all reagents were obtained from ThermoFisher Scientific, Waltham, MA, USA.

Drugs

ONC201 (Chimerix, Philadelphia, PA, USA) and paxalisib (Kazia Therapeutics Limited, Sydney, NSW, Australia) were obtained under a materials transfer agreement.

Cell lines

The use of patient derived DIPG neurosphere cell cultures in this study was approved by the Human Ethics Research Committee, University of Newcastle (H-2018-0241). Cell lines (summarized in Table S1) were cultured as previously described (30).

Sensitivity

Drug effect on cellular growth and proliferation was determined using the resazurin cell proliferation assay as previously established (15). Briefly, DIPG cells were seeded at 2.5×10^4 cells/well in a 96-well plate, incubated overnight at 37°C and treated with a 1:2 serial dilution of ONC201 from 150 μM for 96 h. Cells were treated as neurospheres without growth matrix. For low oxygen testing, DIPG

cells were grown in 5% O_2 conditions for at least 1 week before commencement of assays. Plates were read using a Fluostar system at 544/590 nm and values graphed compared to the untreated control.

Annexin-V FITC assay

Cell death was measured using an Annexin-V FITC apoptosis detection kit (BD Biosciences, Sydney, NSW, Australia) as previously established (15). Cells were seeded at a density of 5×10^4 per well in a 96-well plate and were incubated with ONC201, for 96 h before propidium iodide and Annexin V staining as per manufacturer's recommendations. Stained cells were analyzed using a FACS Canto II flow cytometer and data were processed using FlowJo software.

Colony formation assay

SU-DIPG-VI colony forming ability was assessed via soft agar growth matrix colony formation assay as previously described (31). A total of 3,000 SU-DIPG-VI cells/well were plated into the top agar layer of 24-well plates with indicated doses. MTT was used to count proliferative cells after 2 weeks of growth (5% CO_2 conditions). These data were analyzed with ImageJ and are presented as colony number compared to untreated wells, performed in biological triplicate.

Western Blotting

Protein was extracted from DIPG cells using RIPA buffer as per manufacture's recommendations and previously described (32). BCA quantification was performed using a Pierce BCA Protein Assay Kit (Catalogue No. 23227) according to the manufacturer's instructions. Primary antibodies were incubated overnight at dilutions described in Table S2. Secondary horseradish peroxidase (HRP) conjugated antibody (1662408) (Bio-Rad, Hercules, CA, USA) was used at a dilution of 1:5000. Labeled protein bands were imaged using enhanced chemiluminescence (ECL – Classico, Crescendo (Merck KGaA, Darmstadt, Germany)) in combination with a Chemidoc MP Imaging System (Bio-Rad) and data were analyzed using ImageLab software.

Res259 H3 mutation transfection

The human pediatric glioma cell line Res259 (grade II, diffuse astrocytoma) was transfected to express the wildtype or mutated histone H3 forms, using a Cell Line Nucleofector™ Kit V (Lonza, Basel, Switzerland) with 1 µg of the plasmid containing K27M mutated *H3F3A* or *HIST1H3B* gene fused with the *mCherry* gene, and bearing a resistance gene for Hygromycin B. As a control, cells were transfected with a similar plasmid containing the wildtype *H3F3A* or *HIST1H3B* gene. Cells were selected using Hygromycin B and sorted for mCherry expression. Histones PTMs were collected using a histone extraction kit (Abcam ab113476, Cambridge, UK) and analyzed using immunoblotting.

CRIPS-Cas9

A total of 2 x 10^5 cells were seeded in a 6-well plate and incubated overnight. Cells were then replenished with fresh complete media containing 5 µg/mL polybrene (ThermoFisher Scientific). A 250 µL aliquot of lentiviral cocktail containing either Lenti-Cas9-Blast plasmid (SU-DIPG 13; Addgene, Watertown, MA, USA), Lenti-Cas9-2A-Blast (SU-DIPG 36; Addgene) or FUCas9Cherry (DIPG-HSJD-007; Addgene) was supplemented into the cell media and incubated for 72 h. Transduced cells were selectively maintained in complete media containing 10 µg/mL blasticidin (Jomar Life Research, Scoresby, Victoria, Australia) for at least 7 days, or sorted for mCherry expression, prior to experiment. *CLPP, DRD2, TP53*, and non-targeting control (NTC) single guide RNA (sgRNA), cloned into the U6-gRNA/hPGK-puro-2A-BFP vector, were obtained from the Human Sanger Whole Genome Lentiviral CRISPR Library (ThermoFisher Scientific). The details of gRNA sequence for the *CLPP, DRD2*, and *TP53* were as follows: *CLPP*: 5'-GGTGTGGTGACCGCGGGCCTGG -3'*, DRD2*: 5'- GGCAATGATGCACTCGTTCTGG -3'*, TP53*: 5'-CTCGAAGCGCTCACGCCCACGG -3'

A total of 5 × 10^5 Lenti-X HEK29T were seeded in 6-well plates and the following day were transfected with sgRNA plasmids along with the viral packaging plasmids, psPAX-D64V (Addgene) and pMD2.G (Addgene) using Lipofectamine™ LTX Reagent with PLUS™ reagent as per the manufacturer's recommendations. Transfection media was replaced with fresh media after 6 h and incubated for a further 72 h prior to collection of virus-containing media. Viral media was added to 2 × 10^5 Cas9-expressing DMG cells in a 6-well plate in the presence of 1 µg/mL polybrene, centrifuged at 800 x g for 30 min and then incubated for 72 h. Selection of transduced cells using 2 µg/mL of puromycin in fresh media was performed until non-transduced control cells were dead. Heterogenous cell lines were maintained in 2 µg/mL puromycin. For the establishment of single cell clones from the heterogenous population, single BFP positive cells were sorted in 96-well plates containing a 1:1 mixture of conditioned media and fresh media. Single cell clones were expanded and screened using immunoblotting to identify clones with reduced or absent target protein.

Mass Spectrometry

Proteomic analysis was conducted as previously reported (33). Briefly, protein was extracted from DIPG cells using a Na_2CO_3 solubilization method capable of differentiating between soluble and membrane bound proteins. Oasis solid-phase extraction (SPE) columns (Waters, Milford, MA, USA) were blocked using a trypsin digest of bovine serum albumin (BSA) prior to being used to desalt protein extracts. A total of 100 µg of each sample (as determined by Qubit 2.0 Fluorometer quantification) was labelled with TMT 16 plex pro labelling tags (as per Table S3) according to the manufacturer's instructions. Samples were fractionated by offline high-pH reverse phase fractionation using a Dionex Ultra 3000 uHPLC system (Thermo Fisher Scientific) using nano Ease M/Z Peptide CSH C18 column (130 A, 1.7 µm, 300 µm × 100 mm) (Waters). LC-MS/MS was performed using EASY-nLC 1000 (Thermo Fisher Scientific) coupled online to an Orbitrap Exploris

480 mass spectrometer (Thermo Fisher Scientific). Raw files were processed via Proteome Discoverer 2.5.

Hierarchical clustering was performed using Perseus. For our parameters, we used a Euclidean distance, with average linkage and no constraint. A pre-process with k-means was performed, with a maximum of 300 clusters, no more than 10 iterations and 1 restart. Due to the small size of some clusters, we grouped like clusters where the same treatment had similar expression profiles. Cluster 1 was the combination of two clusters, while cluster 3 was the combination of 7 clusters, 4 of which with clusters less than 5 genes. Cluster 2 and cluster 4 are standalone. Hierarchical clustering trees have been highlighted. Ingenuity Pathway Analysis software (IPA; Qiagen) was used for bioinformatic analysis of proteomic dataset. Canonical pathways, and upstream regulator analyses were generated and assessed based on p-value and z-scores.

DIPG xenograft modeling

All *in vivo* experiments were conducted in compliance with the approved CNH Institutional Animal Care and Use Committee protocol (#30425), the University of Newcastle Animal Care and Ethics Committee (#A-2019-900) and the University of California San Francisco Institutional Animal Care and Use Committee (IACUC). Five-week-old, male, NSG mice were implanted with 100,000 SU-DIPG-VI/Luc and 300,000 HSJD-DIPG-007 tumor cells into the pontine region of the brainstem using coordinates with Lambda as the reference point (Y: 1.5 mm, X: 0.8 mm, Z: 5 mm) at a rate of 1 µL/min. Mice were allowed to recover for 4 and 3 weeks, respectively before commencement of treatment.

For SU-DIPG-VI model, ONC201 and paxalisib were administered by oral gavage at 125 mg/kg (PBS) and 10 mg/kg (0.5% methyl cellulose/0.2% Tween 80), respectively, at a frequency of 1 time/week and 3 times/week. Animals were monitored for weight loss (compared to base weight) and clinical signs. Dose holidays were given at 10% weight loss and resumed at 5% weight recovery. Mice were humanely sacrificed when neurological symptoms were observed, or with more than 20% weight loss.

For HSJD-DIPG-007 xenograft model, ONC201 and paxalisib were administered as above, except paxalisib was given twice daily at 5 mg/kg. Mice were treated for 5 weeks. Mice were sacrificed at endpoints as described above.

For the SF8628 study, five to six week-old, female athymic (homozygous, nu/nu) mice were obtained from Harlan-Envigo Laboratory (Livermore, CA, USA). For tumor inoculation 500,000 human SF8628 DIPG cells with the luciferase reporter gene were intracranially implanted into the right pons as previously described (34). Briefly, anesthetized animals received 2 µL of cell suspensions into the right pontine area, with injection coordinates 1 mm to the right from the lambda, top of lamboid suture and 4 mm depth. Treatment initiated at day 14, when

bioluminescence indicated log phase growth. Mice were euthanized when tumor burden reached levels determined by IACUC guidelines.

Tumor size was monitored bi-weekly, using an IVIS-Lumina III imaging system (PerkinElmer, Waltham, MA, USA) for SU-DIPG-VI-Luc. For SF8628, bioluminescence was measuring using an IVIS Lumina imaging station (Caliper Life Sciences, Alameda, CA) (35). Mice were intraperitonially injected with 150 mg/kg of D-luciferin (Gold Biotechnology) and imaged 10 min following D-luciferin injection. BLI signal intensities were quantified using the region of interest feature of Living Image software. BLI signal at each time point was plotted as an average of total flux (photons/sec) for all animals in each group.

In SU-DIPG-VI, following 2 *in vivo* treatments with ONC201, paxalisib or combination, brainstems were resected lysed with RIPA buffer, immunoblotting was then performed as described above. Samples for immunohistochemistry were collected in the middle of the fourth week of treatment in HSJD-DIPG-007 xenograft model and staining was conducted as previously described for H3K27M, Ki67 and SDHA (15). Images were visualized using ImageScope and pixel intensity was quantified using Image J in technical triplicates across three biological replicates.

Patient experience

Written informed consent was obtained from each of the families whose child's data is included in this study. Two children with biopsy/autopsy-confirmed H3K27M, PIK3CA or PIK3R1 mutant DIPG were treated with ONC201 and paxalisib.

DIPG patient at 5 years old was diagnosed in March 2021 with *H3.1K27M, PIK3R1* and *ACVR1* mutations. A biopsy was performed in the two weeks following this diagnosis, with RT started soon after. The combination of ONC201 (15 mg/kg) and paxalisib (27 mg/m^2) was started 3 months following diagnosis and is ongoing.

DIPG patient at 16 years old, was diagnosed with *H3.3K27M, TP53* and *PIK3CA* mutations on the 19th of December 2018, without a biopsy. They began radiation and ONC201 (15 mg/kg) treatment on the 9th of January 2019. ONC201 alone began February 2019. February 2020 saw further progression, with ONC201 and panobinostat (45 mg daily three times per week), stopped 20th of May 2020 at further progression. Re-irradiation and ONC201 began 29th May. ONC201 and paxalisib (27 mg/m^2) dual compassionate use began 22nd of June 2020.

Statistical Analysis

GraphPad Prism 9 software (La Jolla, CA, USA) was used for statistical analyses. Unless otherwise stated, two sample unpaired Student's t-tests or one-way ANOVA was used to determine significant differences between groups. Where samples sizes were smaller, comparing different biological samples, non-parametric tests, one-way ANOVA, and t-tests were used. Survival analysis was

performed using the Log rank test. Values shown are the mean ±SEM. Significance values: *=*p<0.05*, **=*p<0.01*, ***=*p<0.001,* ****=*p<0.0001* are used throughout.

Data availability

Data generated in this study have been included in the article and supplementary material. The proteomics data is deposited to ProteomeXchange via the PRIDE with the dataset identifier PXD036245 (36). All other raw data is available upon request from the corresponding author.

Results

Comprehensive drug profiling predicts reduced sensitivity to ONC201 in *TP53*-mutant DIPG

Using fourteen patient-derived neurosphere-cell culture models harboring DMG molecular subtypes (H3-wt n=2, H3.1K27M n=4, and H3.3K27M n=7) and immortalized neural cell controls (HCMEC/D3 blood-brain barrier (BBB) endothelial cells, HMC3 microglial cells and ReN neural progenitor cells), we assessed sensitivity to ONC201 via inhibition of proliferation, induction of apoptosis and cell death. Overall, 43% of DIPG models, showed >50% reduction in proliferation following ONC201 exposure (Fig. 1A, Table S4). However, we identified a subpopulation of DIPG models, including controls, which demonstrated <50% reduction in proliferation, even at very high concentrations of ONC201 (>150 μM) for up to 96 h. (Fig. 1A, Table S4).

Analysis of cell death markers via annexin V/PI cytotoxicity analysis corroborated proliferation data, showing ONC201 is cytotoxic to SU-DIPG-XXXIII (p=0.0043) and HSJD-DIPG-007 (p=0.0018*),* with UON-JUMP4 and SU-DIPG-XIII demonstrating decreased sensitivity (Fig. 1B), akin to previous studies testing ONC201 in DIPG models (15,25) and at physiologically relevant doses (5 μM) (37). Neurosphere morphology was assessed following 6-day ONC201 treatment to account for variations in doubling times (Fig. S1) across eleven DIPG cell line models. ONC201 sensitive cells showed reduced cell number and less viability, while neurosphere models similarly featured less robust sphere formation accompanied by more non-viable, singular cells (Figs. 1C upper panel, S2). By contrast, models with decreased sensitivity retained cell number and neurosphere morphology and presented with fewer differences in non-viable cells compared to untreated controls (Figs. 1C lower panel, S2B).

To determine whether recurring mutations influenced the sensitivity of DIPG cell lines to ONC201, we performed pharmacogenomic analysis using next generation sequencing (summarized in Fig. 1D). As a means of determining the comparative sensitivity across models we calculated the area under the curve (AUC) of cell lines treated with ONC201 (Fig. 1A), and grouped DIPG models by H3K27 status and assessed whether there were differences in sensitivity (Fig. 1E). No difference in ONC201 sensitivity was seen in H3K27-altered subtypes (Fig. 1E, wt-H3 vs. H3.1K27M, p=0.0696; wt-H3 vs. H3.3K27M, p=0.09999; H3.1K27M vs. H3.3K27M, p=0.1711). In line with previous studies of ONC201 efficacy in glioblastoma models (21), and to confirm the role histone mutations may play

in response to ONC201, we knocked in H3.1K27M or H3.3K27M mutations into wt-H3 astrocytoma models (Res259) (38). Res259 cells harbor overexpression of PDGFRA and KIT (39), which represent a similar genetic architecture to DMGs without the H3-/EZHIP- alterations. In line with previous studies Res259-H3.3K27M+ cells showed significantly increased sensitivity compared with H3.1K27M+ cells (H3.3K27M vs. H3.1K27M p=0.0139) (Figs. 1F,G, S3A,B).

Besides H3K27M-alterations, *TP53* loss of function mutations (LoF) were the next most frequently identified in our DIPG models (n=9), and included missense variants (n=5), stop gains (n=3) and a splice donor variant (n=1), predominantly affecting H3.3K27M DIPG models (Fig. 1D). *TP53*-mutant DIPG models were significantly less sensitive to ONC201 than wt-*TP53* DIPG models (p = 0.014) (Fig. 1H). Receiver operating characteristic (ROC) curve analysis supported the pharmacogenomic observation that *TP53*-mutant DIPGs possessed decreased sensitivity to ONC201 (AUROC=0.9722, p=0.0087) (Fig. S3C). To further explore the influence of *TP53* mutations, we performed CRISPR-Cas9 mediated *TP53* knockdown (KD) and single cell knockout (KO) using the ONC201 sensitive HSJD-DIPG-007 DIPG model, which harbors wt-*TP53*, H3.3K27M and mutant *PPM1D* (Fig. 1A,B,D). Modulating expression of *TP53* did not influence proliferation rate (Fig. S3D), however, in agreement with our pharmacogenomics studies, *TP53* KD/KO decreased sensitivity of HSJD-DIPG-007 to ONC201 treatment compared to non-targeting gRNA controls (NTC) (ONC201 IC_{50} wt-*TP53*=2.202 μM, *TP53*-KD=7.344 μM p=0.0117, *TP53*-KO=NR p=0.004) (Figs. 1I,J, S3E). The role LoF *TP53* mutations in response to ONC201 was further investigated using immunoblotting, which demonstrated that 5 μM ONC201 induced robust cleavage of PARP, indicative of apoptosis in wt-*TP53* cells, moderate cleavage in *TP53*-KD cells, but no cleavage of PARP in *TP53*-KO HSJD-DIPG-007 cells (Fig. 1K), corroborating the pharmacogenomic analysis showing that DIPG cells harboring *TP53* mutations show decreased sensitivity to ONC201. Using the small molecule MDM2 inhibitor of Nutlin-3, we show that knockdown/knockout of *TP53* mimics LoF mutations, driving senescence only in non-transfected control (*TP53*-NTC IC_{50} = 3.507; *TP53*-KD and *TP53*-KO IC_{50} = NR) than *TP53*-KD and *TP53*-KO, which did not reach IC_{50} (Fig. 1L). Further, even though HSJD-DIPG-007 cells harbor a *PPM1D* mutation, these cells are as sensitive to MDM2 antagonism in line with other *PPM1D* mutant cells lines, (40) and conversely to HSJD-DIPG-007 cells harboring *TP53* LoF, show reduced sensitivity to ONC201 (Figs. 1L, S3F,G). As *TP53* and H3.3K27M mutations are known to associate with aneuploidy, and a chromosomal instability signature, we examined if *TP53* mutations and ONC201 sensitivity correlated with chromosomal instability (41), through the measurement of tumor mutational burden (TMB), microsatellite instability (MSI) (Figs. 1D, S3H,I) and chromosomal gains and losses (Fig. S3J,K). No difference between *TP53* status and MSI, TMB or chromosomal gains/losses was observed, suggesting this may not be a feature of *TP53* mutant DMGs in our cohort. Furthermore, TS0-500 revealed high number of *ACVR1*-mutant DIPGs (38%, n=5), often co-occurring with H3.1K27M

(23%, n=3) (Fig. 1D). We next examined whether *ACVR1* promoted sensitivity to ONC201, however showed no difference in ONC201 sensitivity between wt-*ACRV1* and mutant DIPGs (p=0.1274, Fig. 1M). Additionally, as *ACVR1* and *PIK3CA* regularly co-occur (23%, n=3), with recurrent *PIK3CA* mutations seen in our DMG models (31%, n=4), we examined if *PIK3CA* mutations could predict sensitivity and show here that they are more sensitive to ONC201 compared to wt-*PIK3CA* DIPGs (p=0.012, Fig. 1N).

Somatic pharmacogenomic analysis identified DRD2 and CLPP to be targets of ONC201 in DIPG

In vitro profiling of the G-protein coupled receptor (GPCR) superfamily has previously shown ONC201 to be a dopamine receptor (DRD2/3/4) antagonist (24), as well as an agonist of the mitochondrial protease ClpP (19,23). Recently we performed molecular modeling of both ClpP and DRD2 to show that ONC201 binds to both targets with high affinity (15). Therefore, to identify targets of, and hence pathways influenced by ONC201, we correlated ONC201 sensitivity (z-AUC) with basal gene (Fig. S4A) and protein (Fig. 2A) expression profiles of known putative targets. High DRD2 protein expression was significantly correlated with increased sensitivity to ONC201 (R^2=0.2348, p=0.0027) (Fig. 2B), and at the transcript level (R^2=0.1382, p=0.0431) (Fig. S4B). A significant correlation was also identified for ClpP at the protein level (R^2=0.1240, p=0.0352) (Fig. 2B) however, not at the transcript level (R^2=0.06571, p=0.1715) (Fig. S4B). Pediatric HGG patients, including DIPG patients, harbor ubiquitously high-*CLPP* expression, more so than any other pediatric CNS tumor (Fig. 2C) (42). Agonism of ClpP by ONC201, increases its proteolytic activity to drive degradation of respiratory chain complex subunits including Succinate dehydrogenase A and B (SDHA and SDHB), among others (23) (Fig. S4C). Succinate dehydrogenase enzymes form integral components of both the TCA cycle and mitochondrial respiratory ETC, and not only oxidize succinate to fumarate to support energy production, but their loss promotes oxidative stress through the production of ROS and release intermediates that control chromatin modifications and gene expression (43). Our recent study of ONC201 used by DIPG patients, showed ONC201 elicited potent degradation of SDHA in DIPG patient derived xenograft (PDX) tumor tissue *in vivo* (15). Analysis shows that SDHA protein expression did non-significantly correlate with ONC201 sensitivity (R^2=0.05555, p=0.1664) (Fig. 2B), and this was also not at the transcript level (R^2=0.118, p=0.071) (Fig. S4B). However, the ratio of SDHA (proteolytic target) to ClpP (protease) protein expression profiles may influence DMG cell sensitivity to ONC201 (R^2=0.1823, p=0.0094) (Fig. 2B), providing further evidence that ClpP is a target of ONC201 in DIPG. We further examined the role of ClpP and DRD2 in mediating ONC201 sensitivity using CRISPR-Cas9 mediated knockdown (Fig. 2D). Indeed, loss of *CLPP* expression had no effect on the ONC201-cell line harboring reduced sensitivity (SU-DIPG-XIII) yet abrogated the effects of ONC201 in the sensitive line (SU-DIPG-XXXVI) (Fig. 2D,E). Interestingly, DRD2 was shown to be indispensable for DIPG cell line

proliferation *in vitro*, regardless of sensitivity (Fig. 2D,E), analogous to *in vitro* and *in vivo* studies performed in patient derived glioblastoma models (44).

Quantitative proteomic profiling confirms ONC201 drives mitochondrial degradation, rescued by redox-regulated PI3K/Akt signaling

Pharmacogenomics coupled with gene editing predicted *TP53* mutations/LoF to influence sensitivity to ONC201 (Fig. 1), which is at odds with previous studies in non-DIPG cancers (17,22). However, biochemical correlation of putative targets including DRD2 and CLPP supports previously identified mechanisms of the anti-cancer effects of ONC201 in non-DIPG cells.

Given the critical role SDHA plays in mitochondrial respiration, we performed high-resolution quantitative proteomic profiling following ONC201 exposure (5 μM, 24 h) in both normoxic and low oxygen conditions to mimic the spatial heterogeneity of DIPG using SU-DIPG-VI cells (H3.3K27M, *TP53*-mutant, DRD2-low, SDHA-high, ONC201 resistant) (Table S5). Hierarchical clustering revealed subtle but significant changes in protein expression induced by ONC201 treatment in cells grown under different oxygen tensions (Fig. S5A). By interrogating differentially and commonly expressed clusters, assigned using the differences influenced by ONC201 or oxygen concentration (Fig. S5B,C) using Ingenuity Pathway Analysis (IPA), we identified mitochondrial dysfunction as the most significantly altered canonical process across these clusters and across both oxygen tensions following ONC201 treatment (p=1E-27) (Figs. 3A, S5B,D) (Table S6-8), with oxidative phosphorylation the most significantly downregulated cellular process (p=1.58e-24, z-score=-4.49) (Figs. 3A, S5B,C). Activated upstream regulator analysis further revealed the role that ONC201 plays in promoting ClpP (p=6.65E-09, z-score=3.051) and KDM5A (p=2.22E-15, z-score=4.2) activity, disrupting mitochondrial homeostasis (p=6.65E-09, z-score=3.051) (Fig. 3B) and degrading mitochondrial and tricarboxylic acid cycle (TCA) proteins, (SDHA, p=2.58E-04 and IDH3B, p=5.29E-03, respectively), as well as additional enzymes of the mitochondrial energy production pathways (Fig. 3C). Immunoblotting confirmed the changes in protein expression revealed by mass spectrometry, here ONC201 elicited degradation of mitochondrial proteins SDHA and IDH3A/B and increased phosphorylation of H2AX (Fig. 3D).

Protein expression profiles significantly regulated by ONC201 treatment across oxygen tensions predicted the Akt serine/threonine kinase, the key effector of the PI3K pathway, to be up-regulated following ONC201 treatment (AKT1, z-score=2.399; Akt, z-score=2.349), (Fig. 3B) (Table S9). Additionally, IL-15 activity (z-score=2.416), which is known to stimulate the JAK-STAT pathway and PI3K/Akt signaling was predicted to be increased (45). Taken together, the predicted increase of PI3K/Akt signaling is potentially responsible for the significantly altered protein expression profiles seen following ONC201 treatment (Fig. 3E). These include decreased expression of the proapoptotic protein BAD, increased expression of the antiapoptotic protein BCL2 as well as increased expression of markers of quiescence and progenitor cell types such as SOX2 and EZH2.

Predicted increased activity of activating transcription factor 4 (ATF4) (z-score=2.051, *p*=0.0104) (Fig. 3B), leading to anti-apoptosis through unfolded protein response (*p*=5.89E-04) (Fig. S5B) (46) is also driven by increased PI3K/Akt signaling, inferring a mechanism of avoiding cell death processes following ONC201 treatment.

To further elucidate the role PI3K-Akt activation may be playing in resistance to ONC201 we performed high-resolution comparative and quantitative proteomic profiling following ONC201 exposure (5 μM, 24 h) across additional DIPG cell lines with varying sensitivity to ONC201; SU-DIPG-XXXVI, SU-DIPG-XIII and compared to SU-DIPG-VI (Fig. 3F). SU-DIPG-VI and SU-DIPG-XIII cells, less sensitive to ONC201 clustered together, away from SU-DIPG-XXXVI, which is more sensitive to ONC201. Analysis using IPA revealed mitochondrial dysfunction and activation of CLpP/KDM5A following treatment with ONC201 across all cell lines (Fig. 3G), further validating ONC201 to be elucidating anti-DIPG effects through mitochondrial dysfunction. Treatment with ONC201 induced activation of PI3K-Akt signaling proteins (Fig. 3G), including Akt, IGF1 and downregulated PTEN signaling, in all cell lines, suggesting Akt activation is a reciprocal mechanism associated with ONC201 treatment, however greater upregulation of Akt signaling was observed in cell lines less sensitive to ONC201 (z-score: Akt SU-DIPG-XXXVI=1.067, SU-DIPG-VI=1.692, SU-DIPG-XIII=2.039, mTOR: SU-DIPG-XXXVI=0.378, SU-DIPG-VI=1.134, SU-DIPG-XIII=1.890). Given that unbiased global proteomic profiling results predicted increased PI3K/Akt activity following ONC201 exposure, we orthogonally validated phosphorylation changes of proteins regulated by this pathway, all of which showed increased phosphorylation in cells refractory to ONC201 following treatment (Fig. 3H). Activated PI3K/Akt signaling potentiated phosphorylation of Akt at Thr308 and Ser473 across DIPG lines regardless of ONC201 sensitivity, however activation of downstream pathway proteins GSK3α, GSK3β, p70S6K was only present in cell lines showing reduced sensitivity to ONC201 (SU-DIPG-VI, SU-DIPG-XIII and SU-DIPG-XVII) (Fig. S5E). In cell lines more sensitive to ONC201, the increase in Akt phosphorylation occurred earlier (24 h for HSJD-DIPG-007), however after 48 h, these cells became apoptotic as indicated by increased cleaved PARP (Fig. 3H). Such data aligns with our recent demonstration that ONC201 drives mitochondrial ROS production and mitochondrial structural abnormalities (25), and thereby links these responses with the oxidative DNA damage seen in these cells (γH2AX, Fig. 3D).

Together, the increased mitochondrial oxidative stress caused by ONC201's ClpP agonism and electron leakage (25), commensurate with increased PI3K/Akt signaling activity, may be promoting the activity of the stress sensing transcription factor nuclear factor erythroid 2–related factor 2 (NRF2) (Fig. 3G), as increased expression of its downstream target, the reductase NQO1 was detected following ONC201 treatment (log2 fold-change = 0.28, *p*=0.0017 and orthogonally validated) (Figs. 3C,E,H). NQO1 is responsible for promoting redox homeostasis and cell survival (47). In this regard, KEAP1 is known to regulate the activity of NRF2, and is degraded with ONC201

treatment, leading to decreased abundance (Fig. 3H). These observations are in line with previous studies that show loss of expression/degradation of KEAP1 promotes the transcriptional activity of NRF2 resulting in partial epithelial to mesenchymal transition but only in tumors harboring *TP53* LoF mutations (48). These observations potentially explain the persistent proliferation of *TP53*-mutant DIPG cells even in the presence of high dose ONC201.

ONC201 driven oxidative stress drives PI3K/Akt signaling highlighting the potential of ONC201 combined with the PI3K/Akt inhibitor paxalisib

Proteomic profiling predicted that increased PI3K/Akt signaling may be leading to decreased sensitivity of DIPG cells to ONC201 (Fig. 3). Previously we showed ONC201 increased ROS production (25) therefore, we used the potent ROS scavenger *N*-acetyl-l-cysteine (NAC) to investigate whether there was a link between increased ROS and increased PI3K/Akt signaling. NAC abrogated phosphorylation of Akt, while hydrogen peroxide (H_2O_2) increased phosphorylation (Figs. 4A, S6A,B). As such, we hypothesized that inhibition of PI3K signaling may prevent the Akt-mediated cell survival signaling induced following exposure to ONC201. To investigate this, we tested whether the brain penetrant PI3K/Akt inhibitor paxalisib (previously GDC-0084) (28,29) could also suppress PI3K/Akt signaling in response to ONC201. Paxalisib decreased phosphorylation of Akt in the H3.3K27M, *TP53*-mutant and ONC201-refractory model SU-DIPG-XVII either alone or in combination with ONC201 (Fig. 4B) (49). Again, ONC201 modulated the abundance of proteins mapping to NRF2 regulated antioxidant response including the loss of KEAP1, increased NQO1, both abrogated by the combination with paxalisib (Fig. 4B) to drive cell death.

To assess adhesion-independent cell proliferation and survival of DIPG cells treated with ONC201 we performed soft agar colony forming assays using SU-DIPG-VI that show decreased sensitivity to ONC201 as a monotherapy. Encouragingly, at physiologically relevant dosing, single agents decreased colony formation (ONC201 -0.43 $\log_2$ fold, p=0.007; paxalisib -0.5 $\log_2$ fold, p=0.0032*),* with the combination of ONC201 and paxalisib significantly decreasing colony formation beyond that achieved using either of the single agents (combination vs. UT, -1.4 $\log_2$ fold, p=<0.0001, combination vs. ONC201, -1 $\log_2$ fold, p=0.0007, combination vs. paxalisib, -0.93 $\log_2$ fold, p=0.0014) (Fig. 4C). Indeed, ONC201 in combination with paxalisib synergized, particularly in H3.3K27M *TP53*-mutant DIPG models, regardless of whether the treatment was performed under normoxic or low oxygen conditions (Figs. 4D,E, S7, S8A,B, Table S10), however, the combination was additive in the UON-JUMP4 model, grown in low oxygen conditions (Fig. S8A,B). As an additional control, we assessed the sensitivity of human peripheral blood mononuclear cells *in vitro* donated from healthy volunteers to each drug individually and in combination, which revealed no increase in cell death; however, a reduction in PI3K/Akt/mTOR signaling was observed (Fig. S8C,D).

To determine if *TP53* status influenced ONC201 PI3K/Akt signaling we investigated the effect of ONC201 in the *TP53*-KD and *TP53*-KO HSJD-DIPG007 models via immunoblotting. Here, ONC201 decreased SDHA abundance and ERK1/2 phosphorylation regardless of p53 status (Fig. 4F). Again, ONC201 significantly increased phosphorylation of Akt at both T308 and S473 residues (Figs. 4F, S9) across models, including cells harboring either *TP53*-KD or *TP53*-KO. Interestingly, *TP53*-KD and *TP53*-KO HSJD-DIPG-007 cells harbored significantly increased basal levels of phosphorylation of Akt at T308, a marker of active PI3K signaling compared to the NTCs, which was further potentiated using ONC201 (Figs. 4F, S9). Therefore, to determine whether paxalisib could rescue the decreased response promoted by KD and KO of *TP53* in HSJD-DIPG-007 cells we tested ONC201 in combination with paxalisib and identified very high-level synergy in the *TP53*-KD / *TP53*-KO cells, greater than three times that of parental cells and corresponding to the level of increased PI3K signaling seen (Figs. 4G,H, S10). Together, these *in vitro* results highlight the potential for the use of paxalisib in combination with ONC201 even in highly aggressive H3.3K27M *TP53*-mutant DIPG models.

Preclinical optimization of ONC201 combined with paxalisib

Clinical trials testing ONC201 and paxalisib as monotherapies in DIPG/DMG have demonstrated acceptable safety and toxicity profiles (NCT03416530 and NCT03696355, respectively). Therefore, to test the preclinical utility of ONC201 combined with paxalisib we first examined their efficacy using the SU-DIPG-VI-Luc (H3.3K27M, *TP53*-mutant) and HSJD-DIPG-007 (H3.3K27M*, TP53*-wildtype) DIPG xenograft mouse models, using mouse equivalent MTDs (125 mg/kg q.w. ONC201, in combination with paxalisib 10 mg/kg t.i.w., or 5 mg/kg/b.i.d., respectively) (42,43), engrafted into the fourth ventricle/pons of NSG mice (Fig. 5A). SU-DIPG-VI-Luc mice were treated continuously and HSJD-DIPG-007 mice were treated for five weeks from treatment start (Fig. 5A). *In vivo* bioluminescence imaging (BLI) was performed immediately before drug or vehicle control administration to assess baseline tumor burden (Fig. S11A,B). Using BLI as a surrogate for tumor size in SU-DIPG-VI-Luc, ONC201 had no significant effect on tumor size, while paxalisib significantly reduced tumor burden (paxalisib=404.84 p sec^{-1} cm^{-2} sr^{-1}, p=0.0309) (Fig. S11A,B). ONC201, combined with paxalisib, decreased tumor burden throughout the treatment regimen compared to vehicle control (4-week mean BLI ONC201+paxalisib=158.34 p sec^{-1} cm^{-2} sr^{-1}, p=0.0038).

Both ONC201 and paxalisib as single agents significantly extended the survival of SU-DIPG-VI-Luc xenograft models compared to vehicle controls, with the combination significantly extending the survival compared to all treatments (vehicle=45 days, ONC201=56 p=0.0082, paxalisib=54 days p=0.0082, ONC201+paxalisib=72 days, combination *vs*. vehicle p=0.0027, combination *vs*. paxalisib p=0.0198, and combination *vs.* ONC201 p=0.0044, post treatment start) (Fig. 5B) (50). In the SU-DIPG-VI model, we identified some early toxicity using 10 mg/kg/day (Fig. S11C), therefore, treated

HSJD-DIPG-007 mice with 5 mg/kg/b.i.d. to improve tolerability (Fig. S11D). In the ONC201 sensitive, HSJD-DIPG-007 model, ONC201 provided an increased survival (vehicle=43.5 vs. ONC201=50 days, p=0.0009), and twice daily low dose paxalisib also provided an improved survival advantage (vehicle vs. paxalisib=55 days, p<0.0001) (Fig. 5C). Together the combination both significantly increased survival effect vs. controls (combination=61 days, p<0.0001) and was synergistic compared to monotherapies (ONC201 vs. combination, p=0.0003; paxalisib vs. combination, p=0.0019) (Fig. 5C). Analogous to *in vitro* studies (Fig. 4), tumors resected from SU-DIPG-VI-Luc+ DIPG xenograft mice treated for two weeks, showed increased Akt phosphorylation and expression of EZH2 following ONC201 treatment alone, consistent with our *in vitro* proteomic profiling, with the former rescued using paxalisib (Fig. 5D). To determine whether systemic effects of ONC201 treatment *in vivo*, we measured the expression of tyrosine hydroxylase (TH) (Fig. 5E). ONC201 treatment decreased TH expression in the prefrontal cortex, but not in brainstem where the SU-DIPG-VI cell line was engrafted (Fig. 5E). ONC201 decreased ERK phosphorylation in both the prefrontal cortex and brainstem (Fig. 5E), commensurate with global effects on DRD2 inhibition, suggesting that systemic effects of DRD2 inhibition and ERK phosphorylation may contribute to efficacy observed in these models. To assess pharmacodynamic markers of treatment response, we performed immunohistochemistry on fixed tumor tissue following 4 weeks of treatment. Tumor was detected in the pons of all animals; however, compared to the controls, decreased H3K27M staining was seen across biological replicates, including in the cerebellum of treated mice (Fig. 5F,G) (p<0.05). Compared to the controls, decreased staining of the proliferation marker Ki67 was also seen across treatments (ONC201, p=0.0114; paxalisib, p=0.0023; combination p=0.0002), with the combination also significantly decreased compared to ONC201 alone (p=0.0275) (Fig. 5F,G). Significantly decreased staining for SDHA was seen in samples treated with ONC201 and the combination (ONC201, p=0.008; ONC201+paxalisib, p=0.0436, respectively) (Fig. 5F,G).

Using the highly aggressive H3.3K27M+ SF8628 DIPG xenograft model (51), paxalisib alone and the combination of ONC201 and paxalisib decreased tumor burden at early timepoints (Day 4; vehicle vs. paxalisib, p=0.0075, vehicle vs. combination p=0.0152, Day 10; vehicle vs. paxalisib, p=0.0042, vehicle vs. combination p=0.0032) (Fig. S11E), commensurate with survival analysis, where paxalisib alone provided a significant survival benefit compared to the vehicle (vehicle=22.5 days, paxalisib=28 days, p=0.0453) as did the combination therapy (ONC201+paxalisib=28 days, p=0.0002) (Fig. S11F). The combination of ONC201 and paxalisib also increased survival of xenograft mice compared to ONC201 alone (p=0.0024), and provided a modest benefit compared to paxalisib alone (p=0.0442) (Fig. S11F).

Case reports of ONC201 combined with paxalisib in DIPG patients at diagnosis or disease progression

To demonstrate the potential utility of ONC201 in combination with paxalisib, we report two recent DIPG case studies of patients that received both ONC201 and paxalisib through compassionate access. These patients underwent radiographic analysis according to response assessment in pediatric neuro-oncology (RAPNO). The first is a 6-year-old patient diagnosed in March 2021, harboring H3.1K27M, *ACVR1* and *PIK3R1* mutant DIPG identified following biopsy (Fig. 6A). At diagnosis, a diffuse pontine lesion was identified (Fig. 6B,C, tumor area 1554 mm^2). The patient received 54 Gy of RT delivered in 30 fractions of 1.8 Gy in the 1-3 months following diagnosis. Post-RT magnetic resonance images (MRIs) indicated a tumor reduction of 38.1% compared to diagnosis (Fig. 6B,D, tumor area 962 mm^2). The patient began the combination treatment of ONC201 (15 mg/kg q.w.) and paxalisib (27 mg/m^2 daily) 7 weeks following the post-RT scan, corresponding to 5 months post-diagnosis. Tumor size remained relatively stable over the next consecutive MRIs (Fig. 6E,F, tumor area=1156 mm^2 and 1224 mm^2, respectively). Encouragingly, 9 months post-diagnosis, a substantial 62.1% decrease in tumor area based on T2 weighted images was recorded from the previous MRI, representing a 70.1% reduction compared to diagnosis and 51.8% reduction compared to post-RT (Fig. 6B,G, tumor area=464 mm^2), showing a partial response. Furthermore, 12 months post-diagnosis, 8 months into the ONC201 and paxalisib combination, the tumor had reduced by 80.3% and 68.2%, compared to diagnosis and post-RT, respectively (Fig. 6B,H, tumor area=306 mm^2). Clinically, twenty-four months post-diagnosis, the tumor remains stable (Fig. 6I) and the patient continues to do well, experiencing continued reduction in DIPG associated clinical symptoms, and has returned to school. Intermittent toxicities during treatment included grade II mucositis during the initial few months on the combination, which responded well to dexamethasone mouthwash.

The second DIPG patient was a 16-year-old diagnosed with DIPG (tumor area=977.8 mm^2) (Fig. 6J-L). The patient did not have a biopsy and began radiotherapy in combination with ONC201 (625 mg, q.w.) soon after diagnosis. The patient then continued to receive ONC201 as a maintenance therapy. Clinical and radiological signs of first progression were detected 15 months post-diagnosis (Fig. 6K,M, tumor area=1303.3 mm^2). The patient then received the combination of ONC201 and panobinostat (45 mg daily three times per week) but stopped after 3 months upon detection of further signs of disease progression (Fig. 6K,N, tumor area=1814 mm^2). The patient then immediately underwent re-irradiation (20 Gy delivered in 10 x 2 Gy fractions). Paxalisib (45 mg, 27 mg/m^2) was then combined with ONC201 (625 mg) 18 months post-diagnosis and continued until the patient succumbed to Pneumocystis pneumonia (PCP), 24 months post-diagnosis. The acquired PCP was attributed to concomitant steroid use and hence, the patient was unable to continue either therapy, ultimately passing away 6 months after re-irradiation. T2 axial MR scans during ONC201 and paxalisib treatment showed partial response, with a 34% reduction in total tumor area compared to regression (Fig. 6N to Fig. 6P) and 9% reduction during treatment with ONC201 and

paxalisib (Fig. 6O to Fig. 6P), a reduction not seen when ONC201 was combined with RT at diagnosis (Fig. 6K,O,P). Autopsy analysis revealed viable tumor with no evidence of growth when compared with the latest MRI 1 month earlier, with the family of the child also reporting no signs of DIPG associated clinical symptoms prior to the infection. NGS of post-mortem tumor tissue identified typical H3.3K27M, *TP53*, *PIK3CA* mutations (Fig. 6J), highlighting the potential of combined use of ONC201 and paxalisib for the treatment of DIPG at diagnosis and disease progression.

Discussion

The recent development and sharing of patient-derived models has helped to illustrate the high level of inter- and intra-tumoral heterogeneity of DIPG and DMG, results that highlight the need for combined therapies that target the metabolic rather than the genomic/epigenetic heterogeneity of the disease (6,13). In this study, we have employed a pharmaco-proteogenomic approach to inform a combination treatment regimen to improve response to the imipridone, ONC201, and build upon the preliminary promising efficacy of the drug for the treatment of DIPG (15,21).

ONC201 is currently being assessed in 12 clinical trials worldwide, including in H3K27-altered gliomas (NCT03295396, NCT03416530 and NCT02525692) which reveal a preliminary survival benefit (27). ONC201 increased median OS for H3K27M brainstem tumor patients (DIPG) to 20 months (p=0.0002), from the historical 11.9 months. Patients who received ONC201 outside of trials purchased by their families from a German oncologist survived 18 months, while those who also underwent re-irradiation survived 22 months (15,52). Although these preliminary results are favorable, patients still succumb within 18-20 months, with some patients failing upfront treatment, indicating mechanisms of intrinsic resistance. Here, we present evidence that decreased response is influenced by PI3K/Akt signaling; prompting us to test the clinically relevant PI3K/Akt inhibitor, paxalisib (NCT03696355) (28,49), both in DIPG cell line models that were sensitive and resistant to ONC201. Combined treatment with ONC201 and paxalisib rescued the therapeutic potential of ONC201 in refractory models, independent of the availability of oxygen and independent of *TP53* status, highlighting the potential for this drug combination therapy to combat the metabolic, spatial and genetic heterogeneity of DIPG. Commensurate with these *in vitro* discoveries, combined treatment tested in two out of three DIPG xenograft models significantly extended the survival of mice compared to monotherapies, while the combination had an additive effect in the other.

We show ONC201 targets DRD2 and ClpP in DIPG models *in vitro* and xenograft models *in vivo*. DIPG models harboring *TP53* mutations show decreased sensitivity to ONC201. This is distinct from previous studies revealing ONC201 to be effective in *TP53*-mutant non-DIPG cancer models (17). Irrespective of sensitivity, ONC201 elicits potent agonism of the mitochondrial protease, ClpP, which drives mitochondrial degradation and ROS production. Previous studies showed ONC201 to be a

selective antagonist of DRD2 and DRD3, causing cell death through tumor necrosis factor (TNF)-related apoptosis-inducing ligand (TRAIL) signaling (22). Overexpression of DRD2 has been correlated with ONC201 sensitivity (53), with antagonism shown to decrease the pro-proliferative effects of DRD2 signaling in glioblastoma, mediated, in part, by Ras/Erk, confirmed in DMG cell lines *in vitro* (15). This mode of action is in agreement with the DRD2 antagonist activity of haloperidol, an FDA approved antipsychotic, which also decreased Erk activity, analogous to the response of DIPG cells that are refractory to ONC201 (15), while having no effect on Akt. The importance of DRD2 antagonism was further highlighted following CRISPR-Cas9 mediated DRD2 knockdown, a strategy that proved lethal to DIPG cells *in vitro*. In several DIPG cell line models, including SU-DIPG-VI, ONC201 showed limited cytostatic effects; however, when the same cell line was implanted into the brainstem of mice, ONC201 provided a significant survival advantage compared to controls. It is plausible that these *in vivo* results reflect ONC201's role in global DRD2 antagonism rather than in the tumor alone. DIPG synthesize and secrete dopamine, a characteristic that is likely supportive of DIPG gliomagenesis (54). In glioblastoma, elevated DRD2 expression is seen in glioma-initiating cell populations, with stimulation causing neuron-like hyperpolarization exclusively driving sphere-formation and increasing tumor engraftment in PDX models (47). Here we observe that treatment of mice with ONC201 decreased expression of tyrosine hydroxylase (TH) in the prefrontal cortex suggestive of global antagonism of DRD2, however, further mechanistic insights are needed to elucidate the anti-tumor benefit in DMGs at this time. It is highly probable that paracrine dopamine signaling also occurs in DIPG as these cells express TH, analogous to electrochemical communications between DIPG and neurons transmitted through synapses to drive proliferation, differentiation, and survival (55). It was recently shown that DIPG patients with increased ^{18}F-DOPA uptake during MRI showed decreased sensitivity to radiotherapy (p=0.001) and experienced worse outcomes independently correlating ^{18}F-DOPA uptake with OS (54). These studies highlight the potential benefit in assessing ^{18}F-DOPA during routine MRI monitoring of patients receiving ONC201 and may contribute to predicting response to ONC201.

Our studies support the findings that ClpP is an important target of ONC201 in DIPG, where agonism caused mitochondrial dysfunction (22), and *CLPP* knockdown abrogated ONC201's anti-DIPG effects *in vitro* (24). Regardless of sensitivity, ONC201 drives oxidative stress (24) (following ClpP-mediated degradation of SDHA, IDH3B, CLS, COX4LI1, COX5A, and COX10), however in non-sensitive cells, promotes redox activation of PI3K/Akt, however the mechanism promoting reduced sensitivity in *TP53*-mutant lines remains unknown. Akt inactivates GSK3α/β a well-characterized mechanism of metabolic rescue driven by increased glycogen and protein synthesis to promote cell survival (49). GSK3α/β also cooperates with Kelch-like ECH-associated protein 1 (KEAP1) (50) to repress the activity of the transcription factor, NRF2 (*NFE2L2)*. Yet under mitochondrial and oxidative stress, KEAP1 is degraded and NRF2 translocates to the nucleus,

binding to the antioxidant response elements at gene promoters to combat oxidative stress, by promoting expression of the two-electron reductase NQO1 (38), this response could be inhibited through the combination with paxalisib to drive cell death. Here we show that *TP53*-KO in HJSD-DIPG-007 leads to increased phosphorylation of Akt at Thr308 and Ser473, further promoting expression of NQO1 in line with this proposed mechanism of action. Additionally, treatment with ONC201 increases phosphorylation of Akt at Thr308 and Ser473 further promoting expression of NQO1. It is important to note that the DIPG xenograft mouse survival benefit provided by the combination was modest, commensurate with the insidious clinical journey experienced by DIPG patients. Early clinical experience from the two cases we report using ONC201 in combination with paxalisib is promising. Both patients demonstrated resolution of clinical symptoms and radiographic tumor regression. The first patient, who demonstrated the more dramatic response and continual regression of the primary tumor extending >18 months post-diagnosis, remains on the combination at the time of submission. Additionally, this strategy was also used in a H3.3K27M, *TP53*, *PIK3CA* mutant DIPG patient enrolled on the phase I clinical trial (NCT03416530) testing oral ONC201 in pediatric patients with newly diagnosed DIPG, experiencing an almost complete regression of the progressive tumor to initial diagnosis size and a reversal of clinical symptoms, regression not seen following upfront RT+ONC201, although the re-RT might have contributed to this response. Both patients tolerated the treatments well by combining treatment with dexamethasone mouthwash. The optimal dose and timing of the combination and whether these enhance the effects of standard of care RT either in the upfront or relapse setting remain to be determined, given that both patients also received either upfront radiotherapy or re-irradiation, respectively. However, in this study we cannot explicitly rule out the contribution of paxalisib to patient response as both patients commenced ONC201 before or at the same time as paxalisib, further, the contribution of paxalisib for patients harboring PI3K mutations has not yet been determined; questions that will be elucidated under clinical trial conditions. Additionally, the off-target effects of paxalisib are currently unknown.

We acknowledge that ONC201 in combination with paxalisib may not be solely responsible for the almost complete resolution of the disease, particularly at advanced stages, given the modest xenograft results using immune-compromised mouse models. Indeed, H3K27M DIPG are known to reside in an immunologically cold tumor microenvironment (TME) devoid of inflammatory immune cells (7). The global loss of the H3K27me3-mediated epigenetic landscape within DIPG cells is similar to those seen in embryonic stem cells (ESCs) (56) characterized by little to no expression of the major histocompatibility complex I (MHC I) proteins, making these primitive cells less visible to the immune system (57). The observed change in the epigenetic landscape following ONC201 treatment and following modulation of oxidative stress may play a role in the immunogenicity of DIPG, particularly in patients with an active immune system. The partial restoration in H3K27me3 following ONC201 treatment is consistent with recent data showing that H3K27M mutations drive

TCA cycle protein expression (58). Here we show that ONC201 drives potent degradation of IDH3A/B and hence loss of mitochondrial TCA cycle function. This, in turn, may modulate the production of epigenetic cofactors required to maintain hypomethylation of H3K27me3 (59). This highlights the emerging link between H3K27M mutations and metabolic and epigenetic plasticity (58), which may play a role in the immunogenicity of the tumor, driving an anticancer response from the immune system.

The preclinical and clinical data provided here underpins the recently commenced phase II clinical trial (NCT05009992), where we are seeking to determine if ONC201 in combination with paxalisib is an effective regimen for treating DIPG and DMG patients at diagnosis, post-RT and at the time of progression when patients are eligible for re-irradiation. This multimodal clinical trial will assess safety of single agents in combination with upfront radiotherapy or re-irradiation for patients commencing the trial at advanced stages that we hope will form the backbone of future combination studies. We hypothesize that rationally designed combination trials, informed by rigorous preclinical data, will improve outcomes for these poor prognosis cancers. Integration of correlative studies will be critical for assessment of predictive biomarkers of response and refinement of inclusion and exclusion criteria for specific combination therapies.

Acknowledgements

We acknowledge all children and their families diagnosed with DIPG. We thank Prof Michelle Monje and Prof Angel Carcaboso for their generous gift of their DIPG cell line models. MDD is supported by a ChadTough Defeat DIPG New Investigator Grant and an NHMRC Investigator Grant – GNT1173892. The contents of the published material are solely the responsibility of the research institutions involved or individual authors and do not reflect the views of NHMRC. This project was supported by the ChadTough Defeat DIPG Foundation, RUN DIPG Ltd, Strategic Group, McDonald Jones Foundation, Vinva Foundation, PNOC Foundation, Yuvaan Tiwari Foundation, Kiriwina Investments, The Kids' Cancer Project, The DIPG Collaborative including: The Cure Starts Now Foundation, The Cure Starts Now Australia, Brooke Healey Foundation, Wayland Villars Foundation, ChadTough Foundation, Aidan's Avengers, Austin Strong, Cure Brain Cancer, Jeffrey Thomas Hayden Foundation, Laurie's Love Foundation, Love Chloe Foundation, Musella Foundation, Pray Hope Believe, Reflections Of Grace, Storm the Heavens Fund, Aubreigh's Army, Whitley's Wishes, Ryan's Hope, Benny's World, The Isabella and Marcus Foundation, Lauren's Fight for Cure, Robert Connor Dawes Foundation, The Gold Hope Project, Julia Barbara Foundation, Lily Larue Foundation, American Childhood Cancer Organization, RUN DIPG, Gabriella's Smile Foundation, and Snapgrant.com, Charlie Teo Foundation, Little Legs Foundation, Tour de Cure, Fight on the Beaches, John Hunter Hospital Charitable Trust, Edie's Kindness Project, Liv Like A Unicorn Foundation, Maitland Cancer Appeal Committee Limited, BlackJack

Pastoral Company, The Hirsch Family Funderpants, and the Hunter Medical Research Institute. Kazia Therapeutics provided funding to support personnel of MDD's laboratory. With thanks to the Isabella and Marcus Foundation, ERJ and SG are supported by the Miette Skiller Scholarship Fund (Josephine Dun and Elliot Gautsch Scholars, respectively) a sub-fund of the Australian Communities Foundation. ERJ is supported by a HCRA Scholarship. RJD is supported by a ChadTough Defeat DIPG Foundation Postdoctoral Fellowship. MLG, AR, SM & EP received funding from "Association Wonder Augustine" & "Association Warrior Enguerrand" for their DIPG studies, MLG is supported by a post-doctoral fellowship from the French ARC Foundation. SP is supported by a Children's Cancer Foundation/Hudson Institute Scholarship; WCC is supported by a Monash University Postgraduate Award; JEC is supported by a Victorian Cancer Agency Mid-Career Fellowship (MCRF17014). NGG is supported by the Perth Children's Hospital Foundation Stan Perron Chair in Pediatric Oncology and Hematology. We would also like to acknowledge support from the Zero Childhood Cancer Initiative, Children's Cancer Foundation and Bailey's Day. FVM is supported by the Cancer Institute NSW Fellowship CDF181218. JRH is supported through grants from the McClurg and Hospital Research Foundations. The clinical trial is supported by Mithil Prasad Foundation, ChadTough Defeat DIPG Foundation and Storm the Heavens, the last also supporting SM. Proteomics was facillitated by NDS from The Analytical and Biomolecular Research Facility, and The Academic and Research Computing Support (ARCS) team, within IT Services at the University of Newcastle, who provided high performance computing (HPC) infrastructure for bioinformatics analyses. Histology services were provided by Cassandra Griffin, Fiona Richards, Megan Clarke and Kaylee O'Brien from the HMRI Core Histology Facility. Immunohistochemistry optimisation and staining services were provided by The University of Newcastle's 'NSW Regional Biospecimen & Research Services', with support from NSW Health Pathology. Figures were created with the assistance of BioRender.com.

Author contributions

E.R. Jackson: Investigation, formal analysis, writing – original draft, writing – reviewing and editing, visualization, **R.J. Duchatel:** Investigation, formal analysis, writing – original draft, writing – reviewing and editing, visualization, supervision, **D. Staudt:** Investigation, formal analysis, writing – reviewing and editing, **M.L. Persson:** Investigation, **A. Mannan:** Investigation, **S. Yadavilli:** Investigation, **S. Parackal:** Investigation, **S. Game:** Investigation, **W. Chin Chong:** Investigation, **W.S.N. Jayasekara:** Investigation, **M. Le Grand:** Investigation, writing – reviewing and editing, **P.S. Kearney:** Investigation, **A.M. Douglas:** Project administration, **I.J. Findlay:** Investigation, formal analysis, **Z.P. Germon:** Investigation, **H.P. McEwen:** Investigation, **T.S. Beitaki:** Investigation, **A. Patabendige:** Resources, writing – reviewing and editing, **D.A. Skerrett-Byrne:** Investigation, methodology, writing – reviewing and editing, **B. Nixon:** Methodology, writing – reviewing and editing, **N.D. Smith:** Methodology, **B. Day:** Resources, **N. Manoharan:** Investigation, patient care,

S. Nagabushan: Investigation, patient care, **J.R. Hansford:** Writing – reviewing and editing, **D. Govender:** Investigation, **G.B. McCowage:** Investigation, Writing – reviewing and editing, **R. Firestein:** Writing – reviewing and editing, **M. Howlett:** Writing – reviewing and editing, **R. Endersby:** Writing – reviewing and editing, **N.G. Gottardo:** Writing – reviewing and editing, **F. Alvaro:** Investigation, writing – reviewing and editing, **S.M. Waszak:** Investigation, writing – reviewing and editing, **M.R. Larsen:** Methodology, writing – reviewing and editing, **Y. Colino-Sanguino:** Writing – reviewing and editing, **F. Valdes-Mora:** Writing – reviewing and editing, **A. Rakotomalala:** Writing – reviewing and editing, **S. Meignan:** Investigation, writing – reviewing and editing, **E. Pasquier:** Resources, investigation, writing – reviewing and editing, **N. André:** Writing – reviewing and editing, **E. Hulleman:** Resources, Writing – reviewing and editing, **D.D. Eisenstat:** Writing – reviewing and editing, **N.A. Vitanza:** Resources, Writing – reviewing and editing, **J. Nazarian:** Conceptualization, resources, writing – reviewing and editing, supervision, **C. Koschmann:** Conceptualization, resources, writing – reviewing and editing, supervision, patient care, **S. Mueller:** Conceptualization, resources, writing – reviewing and editing, supervision, **J.E. Cain:** Conceptualization, resources, writing – reviewing and editing, supervision, **M.D. Dun:** Conceptualization, resources, writing – original draft, writing – reviewing, editing, resubmission, methodology, visualization, supervision, funding acquisition.

References.

1. Ostrom QT, Gittleman H, Liao P, Vecchione-Koval T, Wolinsky Y, Kruchko C*, et al.* CBTRUS Statistical Report: Primary brain and other central nervous system tumors diagnosed in the United States in 2010-2014. Neuro Oncol **2017**;19:v1-v88
2. Warren K. Diffuse intrinsic pontine glioma: poised for progress. Front Oncol 2: 205. 2012.
3. Hoffman LM, Veldhuijzen van Zanten SEM, Colditz N, Baugh J, Chaney B, Hoffmann M*, et al.* Clinical, Radiologic, Pathologic, and Molecular Characteristics of Long-Term Survivors of Diffuse Intrinsic Pontine Glioma (DIPG): A Collaborative Report From the International and European Society for Pediatric Oncology DIPG Registries. Journal of clinical oncology : official journal of the American Society of Clinical Oncology **2018**;36:1963-72
4. Sulman EP, Eisenstat DD. World Cancer Day 2021 - Perspectives in Pediatric and Adult Neuro-Oncology. Front Oncol **2021**;11:659800
5. Pincus DW, Richter EO, Yachnis AT, Bennett J, Bhatti MT, Smith A. Brainstem stereotactic biopsy sampling in children. J Neurosurg **2006**;104:108-14
6. Findlay IJ, De Iuliis GN, Duchatel RJ, Jackson ER, Vitanza NA, Cain JE*, et al.* Pharmaco-proteogenomic profiling of pediatric diffuse midline glioma to inform future treatment strategies. Oncogene **2022**;41:461-75
7. Persson ML, Douglas AM, Alvaro F, Faridi P, Larsen MR, Alonso MM*, et al.* The intrinsic and microenvironmental features of diffuse midline glioma: Implications for the development of effective immunotherapeutic treatment strategies. Neuro Oncol **2022**;24:1408-22
8. Khuong-Quang DA, Buczkowicz P, Rakopoulos P, Liu XY, Fontebasso AM, Bouffet E*, et al.* K27M mutation in histone H3.3 defines clinically and biologically distinct subgroups of pediatric diffuse intrinsic pontine gliomas. Acta Neuropathol **2012**;124:439-47
9. Schwartzentruber J, Korshunov A, Liu XY, Jones DT, Pfaff E, Jacob K*, et al.* Driver mutations in histone H3.3 and chromatin remodelling genes in paediatric glioblastoma. Nature **2012**;482:226-31

10. Wu G, Broniscer A, McEachron TA, Lu C, Paugh BS, Becksfort J*, et al.* Somatic histone H3 alterations in pediatric diffuse intrinsic pontine gliomas and non-brainstem glioblastomas. Nat Genet **2012**;44:251-3
11. Antin C, Tauziede-Espariat A, Debily MA, Castel D, Grill J, Pages M*, et al.* EZHIP is a specific diagnostic biomarker for posterior fossa ependymomas, group PFA and diffuse midline gliomas H3-WT with EZHIP overexpression. Acta Neuropathol Commun **2020**;8:183
12. Chan KM, Fang D, Gan H, Hashizume R, Yu C, Schroeder M*, et al.* The histone H3.3K27M mutation in pediatric glioma reprograms H3K27 methylation and gene expression. Genes Dev **2013**;27:985-90
13. Mackay A, Burford A, Carvalho D, Izquierdo E, Fazal-Salom J, Taylor KR*, et al.* Integrated Molecular Meta-Analysis of 1,000 Pediatric High-Grade and Diffuse Intrinsic Pontine Glioma. Cancer Cell **2017**;32:520-37 e5
14. Duchatel RJ, Jackson ER, Alvaro F, Nixon B, Hondermarck H, Dun MD. Signal Transduction in Diffuse Intrinsic Pontine Glioma. Proteomics **2019**;19:e1800479
15. Duchatel RJ, Mannan A, Woldu AS, Hawtrey T, Hindley PA, Douglas AM*, et al.* Pre-clinical and clinical evaluation of German-sourced ONC201 for the treatment of H3K27M mutant diffuse intrinsic pontine glioma. Neuro Oncol Adv **2021**
16. Arrillaga-Romany I, Kurz S, Tarapore R, Lu G, Sumrall A, Butowski N*, et al.* Clinical efficacy of ONC201 in recurrent H3 K277M-mutant diffusse midline glioma patients. Neuro Oncol **2021**
17. Ishizawa J, Kojima K, Chachad D, Ruvolo P, Ruvolo V, Jacamo RO*, et al.* ATF4 induction through an atypical integrated stress response to ONC201 triggers p53-independent apoptosis in hematological malignancies. Sci Signal **2016**;9:ra17
18. Wagner J, Kline CL, Zhou L, Khazak V, El-Deiry WS. Anti-tumor effects of ONC201 in combination with VEGF-inhibitors significantly impacts colorectal cancer growth and survival in vivo through complementary non-overlapping mechanisms. J Exp Clin Cancer Res **2018**;37:11
19. Greer YE, Porat-Shliom N, Nagashima K, Stuelten C, Crooks D, Koparde VN*, et al.* ONC201 kills breast cancer cells in vitro by targeting mitochondria. Oncotarget **2018**;9:18454-79
20. Fang Z, Wang J, Clark LH, Sun W, Yin Y, Kong W*, et al.* ONC201 demonstrates anti-tumorigenic and anti-metastatic activity in uterine serous carcinoma in vitro. Am J Cancer Res **2018**;8:1551-63
21. Arrillaga-Romany I, Chi AS, Allen JE, Oster W, Wen PY, Batchelor TT. A phase 2 study of the first imipridone ONC201, a selective DRD2 antagonist for oncology, administered every three weeks in recurrent glioblastoma. Oncotarget **2017**;8:79298-304
22. Allen JE, Krigsfeld G, Mayes PA, Patel L, Dicker DT, Patel AS*, et al.* Dual inactivation of Akt and ERK by TIC10 signals Foxo3a nuclear translocation, TRAIL gene induction, and potent antitumor effects. Sci Transl Med **2013**;5:171ra17
23. Ishizawa J, Zarabi SF, Davis RE, Halgas O, Nii T, Jitkova Y*, et al.* Mitochondrial ClpP-Mediated Proteolysis Induces Selective Cancer Cell Lethality. Cancer Cell **2019**;35:721-37 e9
24. Madhukar NS, Khade PK, Huang L, Gayvert K, Galletti G, Stogniew M*, et al.* A Bayesian machine learning approach for drug target identification using diverse data types. Nat Commun **2019**;10:5221
25. Przystal JM, Cianciolo Cosentino C, Yadavilli S, Zhang J, Laternser S, Bonner ER*, et al.* Imipridones affect tumor bioenergetics and promote cell lineage differentiation in diffuse midline gliomas. Neuro Oncol **2022**;24:1438-51
26. Pruss M, Dwucet A, Tanriover M, Hlavac M, Kast RE, Debatin KM*, et al.* Dual metabolic reprogramming by ONC201/TIC10 and 2-Deoxyglucose induces energy depletion and synergistic anti-cancer activity in glioblastoma. Br J Cancer **2020**;122:1146-57
27. Kawakibi AR, Tarapore RS, Gardner S, Chi A, Kurz S, Wen PY*, et al.* Hgg-18. Clinical Efficacy of Onc201 in Thalamic H3 K27m-Mutant Glioma. Neuro-Oncology **2020**;22:iii347-iii
28. Duchatel R, Jackson E, Patabendige A, Cain J, Tsoli M, Monje M*, et al.* DIPG-03. TARGETING PI3K USING THE BLOOD BRAIN BARRIER PENETRABLE INHIBITOR, GDC-0084, FOR THE TREATMENT OF DIFFUSE INTRINSIC PONTINE GLIOMA (DIPG). Neuro-Oncology **2019**;21:ii68-ii

29. Wen PY, Cloughesy TF, Olivero AG, Morrissey KM, Wilson TR, Lu X*, et al.* First-in-Human Phase I Study to Evaluate the Brain-Penetrant PI3K/mTOR Inhibitor GDC-0084 in Patients with Progressive or Recurrent High-Grade Glioma. Clin Cancer Res **2020**;26:1820-8
30. Hutcheon K, McLaughlin EA, Stanger SJ, Bernstein IR, Dun MD, Eamens AL*, et al.* Analysis of the small non-protein-coding RNA profile of mouse spermatozoa reveals specific enrichment of piRNAs within mature spermatozoa. RNA Biol **2017**;14:1776-90
31. Khan A, Gamble LD, Upton DH, Ung C, Yu DMT, Ehteda A*, et al.* Dual targeting of polyamine synthesis and uptake in diffuse intrinsic pontine gliomas. Nat Commun **2021**;12:971
32. Dun MD, Anderson AL, Bromfield EG, Asquith KL, Emmett B, McLaughlin EA*, et al.* Investigation of the expression and functional significance of the novel mouse sperm protein, a disintegrin and metalloprotease with thrombospondin type 1 motifs number 10 (ADAMTS10). Int J Androl **2012**;35:572-89
33. Degryse S, de Bock CE, Demeyer S, Govaerts I, Bornschein S, Verbeke D*, et al.* Mutant JAK3 phosphoproteomic profiling predicts synergism between JAK3 inhibitors and MEK/BCL2 inhibitors for the treatment of T-cell acute lymphoblastic leukemia. Leukemia **2018**;32:788-800
34. Aoki Y, Hashizume R, Ozawa T, Banerjee A, Prados M, James CD*, et al.* An experimental xenograft mouse model of diffuse pontine glioma designed for therapeutic testing. J Neurooncol **2012**;108:29-35
35. Ozawa T, James CD. Establishing intracranial brain tumor xenografts with subsequent analysis of tumor growth and response to therapy using bioluminescence imaging. J Vis Exp **2010**
36. Perez-Riverol Y, Bai J, Bandla C, Garcia-Seisdedos D, Hewapathirana S, Kamatchinathan S*, et al.* The PRIDE database resources in 2022: a hub for mass spectrometry-based proteomics evidences. Nucleic Acids Res **2022**;50:D543-D52
37. Arrillaga-Romany I, Odia Y, Prabhu VV, Tarapore RS, Merdinger K, Stogniew M*, et al.* Biological activity of weekly ONC201 in adult recurrent glioblastoma patients. Neuro Oncol **2020**;22:94-102
38. Rakotomalala A, Bailleul Q, Savary C, Arcicasa M, Hamadou M, Huchede P*, et al.* H3.3K27M Mutation Controls Cell Growth and Resistance to Therapies in Pediatric Glioma Cell Lines. Cancers (Basel) **2021**;13
39. Bax DA, Little SE, Gaspar N, Perryman L, Marshall L, Viana-Pereira M*, et al.* Molecular and phenotypic characterisation of paediatric glioma cell lines as models for preclinical drug development. PLoS One **2009**;4:e5209
40. Xu C, Liu H, Pirozzi CJ, Chen LH, Greer PK, Diplas BH*, et al.* TP53 wild-type/PPM1D mutant diffuse intrinsic pontine gliomas are sensitive to a MDM2 antagonist. Acta Neuropathol Commun **2021**;9:178
41. Zhang M, Zhuang G, Sun X, Shen Y, Wang W, Li Q*, et al.* TP53 mutation-mediated genomic instability induces the evolution of chemoresistance and recurrence in epithelial ovarian cancer. Diagn Pathol **2017**;12:16
42. McLeod C, Gout AM, Zhou X, Thrasher A, Rahbarinia D, Brady SW*, et al.* St. Jude Cloud: A Pediatric Cancer Genomic Data-Sharing Ecosystem. Cancer Discov **2021**;11:1082-99
43. Martinez-Reyes I, Chandel NS. Mitochondrial TCA cycle metabolites control physiology and disease. Nat Commun **2020**;11:102
44. Li J, Zhu S, Kozono D, Ng K, Futalan D, Shen Y*, et al.* Genome-wide shRNA screen revealed integrated mitogenic signaling between dopamine receptor D2 (DRD2) and epidermal growth factor receptor (EGFR) in glioblastoma. Oncotarget **2014**;5:882-93
45. Ali AK, Nandagopal N, Lee SH. IL-15-PI3K-AKT-mTOR: A Critical Pathway in the Life Journey of Natural Killer Cells. Front Immunol **2015**;6:355
46. Pallmann N, Livgard M, Tesikova M, Zeynep Nenseth H, Akkus E, Sikkeland J*, et al.* Regulation of the unfolded protein response through ATF4 and FAM129A in prostate cancer. Oncogene **2019**;38:6301-18
47. Tonelli C, Chio IIC, Tuveson DA. Transcriptional Regulation by Nrf2. Antioxid Redox Signal **2018**;29:1727-45

48. Drainas AP, Lambuta RA, Ivanova I, Sercin O, Sarropoulos I, Smith ML*, et al.* Genome-wide Screens Implicate Loss of Cullin Ring Ligase 3 in Persistent Proliferation and Genome Instability in TP53-Deficient Cells. Cell Rep **2020**;31:107465
49. He C, Xu K, Zhu X, Dunphy PS, Gudenas B, Lin W*, et al.* Patient-derived models recapitulate heterogeneity of molecular signatures and drug response in pediatric high-grade glioma. Nat Commun **2021**;12:4089
50. Rose WC, Wild R. Therapeutic synergy of oral taxane BMS-275183 and cetuximab versus human tumor xenografts. Clin Cancer Res **2004**;10:7413-7
51. Mueller S, Hashizume R, Yang X, Kolkowitz I, Olow AK, Phillips J*, et al.* Targeting Wee1 for the treatment of pediatric high-grade gliomas. Neuro Oncol **2014**;16:352-60
52. Andre N, Buyens G, Bouffet E, Walker D, Dun MD. Access to new drugs in paediatric oncology: can we learn from the ongoing ONC201 saga? Lancet Oncol **2023**;24:209-12
53. Kline CLB, Ralff MD, Lulla AR, Wagner JM, Abbosh PH, Dicker DT*, et al.* Role of Dopamine Receptors in the Anticancer Activity of ONC201. Neoplasia **2018**;20:80-91
54. Morana G, Tortora D, Bottoni G, Puntoni M, Piatelli G, Garibotto F*, et al.* Correlation of multimodal (18)F-DOPA PET and conventional MRI with treatment response and survival in children with diffuse intrinsic pontine gliomas. Theranostics **2020**;10:11881-91
55. Venkatesh HS, Morishita W, Geraghty AC, Silverbush D, Gillespie SM, Arzt M*, et al.* Electrical and synaptic integration of glioma into neural circuits. Nature **2019**;573:539-45
56. Harutyunyan AS, Krug B, Chen H, Papillon-Cavanagh S, Zeinieh M, De Jay N*, et al.* H3K27M induces defective chromatin spread of PRC2-mediated repressive H3K27me2/me3 and is essential for glioma tumorigenesis. Nat Commun **2019**;10:1262
57. Drukker M, Katz G, Urbach A, Schuldiner M, Markel G, Itskovitz-Eldor J*, et al.* Characterization of the expression of MHC proteins in human embryonic stem cells. Proc Natl Acad Sci U S A **2002**;99:9864-9
58. Chung C, Sweha SR, Pratt D, Tamrazi B, Panwalkar P, Banda A*, et al.* Integrated Metabolic and Epigenomic Reprograming by H3K27M Mutations in Diffuse Intrinsic Pontine Gliomas. Cancer Cell **2020**;38:334-49 e9
59. Ceccarelli M, Barthel FP, Malta TM, Sabedot TS, Salama SR, Murray BA*, et al.* Molecular Profiling Reveals Biologically Discrete Subsets and Pathways of Progression in Diffuse Glioma. Cell **2016**;164:550-63

Figure captions

Figure 1. DIPG patient derived cell lines show variable response to ONC201 treatment. A, Resazurin proliferation (percentage compared to untreated) after 96 h ONC201 exposure in DIPG patient-derived cell lines; EZHIP+ (circles) = CNMC-XD-760, DIPG-VUMC10; H3.1K27M (squares) = UON-JUMP4, SU-DIPG-IV, SU-DIPG-XXXIII, SU-DIPG-XXXVI and H3.3K27M (triangles) = HSJD-DIPG-007, SU-DIPG-VI, SU-DIPG-XIII, SU-DIPG-XVII, SU-DIPG-XXIV, SU-DIPG-XXV, SU-DIPG-XXIX. Endothelial cell line, HCMEC/D3, SV-40 dependent human microglial line, HMC3 and neural progenitor cell line, ReN cells, were used as controls (diamonds). Values shown as mean +/- SEM (n=3). **B,** Annexin V apoptosis assay after 96 h exposure with 5 μM ONC201 (dark grey) compared to untreated (light grey) in SU-DIPG-XXXVI, HSJD-DIPG-007, UON-JUMP4 and SU-DIPG-XIII. Unpaired t-test, values shown as mean +/- SEM (n=3), $^{**}p<0.01$. **C,** Representative phase contrast images of biological triplicates (n=3) of HSJD-DIPG-007 and SU-DIPG-XIII following 6 days exposure to 1.25 μM ONC201, scale bar = 0.2 mm. **D,** Oncoplot of somatic mutations determined using TSO500. Cell lines ordered from the least to most sensitive to ONC201 exposure (top to bottom). Larger values of microsatellite instability (MSI) and tumor mutational burden (TMB)

are associated with increased pathogenicity. **E,** Proliferation data was grouped by H3 status; wt-H3 (n=5), H3.1K27M (n=4) and H3.3K27M (n=7), and sensitivity to ONC201 was determined by the area under the curve (AUC), ± SEM. Statistical analysis was performed via non-parametric unpaired one-way ANOVA. **F,** Resazurin proliferation, AUC, following ONC201 exposure for 96 h in Res259 cells harboring knock-in of either H3.1K27M or H3.3K27M mutations. Statistical analysis performed via parametric unpaired t-test, with Welch's correction. **G,** Western blot validation of H3K27M knock-in in Res259 cells. **H,** *TP53* status; wt- and mutant-*TP53* (n=4 vs. n=9), and sensitivity to ONC201 was determined by the AUC, with values shown as mean ± SEM. Statistical analysis performed via non-parametric unpaired t-test. **I,** Resazurin proliferation, AUC, following ONC201 exposure in wt-*TP53* HSJD-DIPG-007 DIPG cell lines transduced with a non-targeting control (NTC) gRNA, *TP53*-KD (knockdown) and *TP53*-KO (knockout). Statistical analysis was performed via parametric unpaired one-way ANOVA with Welch's correction. **J,** Western Blot confirmation of TP53 knockout (KO) and knockdown (KD) in HSJD-DIPG-007 cells. **K,** Validation of decreased response to ONC201 in *TP53*-KD or *TP53*-KO HSJD-DIPG-007 cell lines was performed by Western Blot analysis of PARP cleavage (cPARP). **L,** Resazurin proliferation, AUC, following Nutlin-3 exposure for 96 h in HSJD-DIPG-007 NTC, *TP53*-KD and *TP53*-KO. Statistical analysis was performed via parametric unpaired one-way ANOVA with Welch's correction. **M,** Proliferation data was grouped by ACVR1 status; *ACVR1* wildtype (n=8) vs. *ACVR1* mutant (n=5) and **N,** *PIK3CA* status; *PIK3CA* wildtype (n=9) vs. *PIK3CA* mutant (n=4) and compared to AUC following ONC201 exposure. Statistical analysis performed via non-parametric unpaired t-test.

Figure 2. Pharmacoproteogenomic analysis identifies DRD2 and ClpP as targets of ONC201 in DIPG. A, Western blot analysis of basal DRD2, SDHA and CLPP expression across DIPG models. **B,** Densitometry of protein expressions were normalized to DIPG-VUMC10 and compared with the z-AUC (median area under the curve (AUC) for the control cell lines (HMC3, HCMEC/D3, ReN) – AUC of DIPG cells after exposure to ONC201. Pearson's linear regression, accounting for replicates, was used to determine ONC201 sensitivity correlation for DRD2, CLPP, SDHA and the ratio of SDHA to CLPP (SDHA/CLPP). *p<0.05, **p<0.01, ***p<0.001, ns (not significant), (n=12). **C,** *CLPP* RNA expression from RNA-seq data publicly available through St Jude's PeCan database, normalized to FPKM (Fragments Per Kilobase of transcript per Million mapped reads). NBM (normal bone marrow CD34 positive hemopoietic stem cells/mononuclear cells), DIPG (diffuse intrinsic pontine glioma), non-BS-HGG (non-brainstem-high grade glioma, including not otherwise specified), LGG (low grade glioma), MB (medulloblastoma) and BT other (brain tumor other - ependymoma, atypical teratoid rhabdoid tumor, choroid plexus carcinoma, cranio and CNS tumor not specified). Statistical significance determined via one-way ANOVA. **D,** Resazurin proliferation following ONC201 exposure (compared to untreated, 96 h) of CRIPSR-Cas9 mediated knockdown of *CLPP* and *DRD2* was performed in SU-DIPG-XIII (blue) and SU-DIPG-XXXVI (yellow). Values shown as

mean +/- SEM (n=3). **E,** Western blot validation of successful knockdown of CLPP and DRD2 in SU-DIPG-XIII and SU-DIPG-XXXVI.

Figure 3. Quantitative proteomic profiling identifies increased PI3K/Akt signaling in resistant models. High resolution quantitative proteomic profiling was conducted on SU-DIPG-VI, exposed to 5 μM ONC201 for 24 h. Cells were treated in low oxygen (5% O_2, 5% CO_2) and normoxic conditions (20% O_2, 5% CO_2) in biological triplicate. **A,** Major canonical pathways and **B,** activated upstream regulators (determined by Ingenuity Pathway Analysis – IPA) of proteins significantly altered following 5 μM ONC201, regardless of oxygen tension (Student's t-test, $p<0.05$, n=6). **C,** Expression changes of proteins were calculated as log2 fold change and grouped by mitochondrial proteins, transcription factors and proteins markers of apoptosis. Student's t-test of average change, *$p<0.05$, **$p<0.01$, ***$p<0.001$, ****$p<0.0001$. **D,** Orthogonal validation of mitochondrial changes, such as decreased SDHA were analyzed in DIPG cell lines (HSJD-DIPG-007, SU-DIPG-XXXVI, SU-DIPG-VI, SU-DIPG-XIII, SU-DIPG-XVII) via Western blot, exposed to 5 μM ONC201 for up to 48 h. **E,** Network of proteins from upregulated PI3K/Akt signaling predicted by IPA were integrated in Cytoscape StringApp. Predicted increase (orange) and predicted decrease (blue) functional networks indicated with sharp and dark lines linking proteins to indicate a higher confidence interval. Protein expression changes mapped as $\log_2$ fold change of ONC201/untreated calculated using the right-tailed Fisher Exact Test with the smaller the *p*-value, the more likely the association between proteins not to be a random event ($p<0.05$). **F-G,** High resolution quantitative proteomic profiling was conducted on SU-DIPG-XXXVI, SU-DIPG-VI and SU-DIPG-XXXVI, exposed to 5 μM ONC201 for 24 h. **F,** Heatmap and unbiased hierarchical clustering of protein expression values normalized using z-score of abundances in Perseus. **G,** Canonical pathways and predicted upstream regulators determined by IPA analysis of proteins altered following ONC201 exposure. Positive z-score value is predictive of pathway activation, whereas a negative z-score is predictive of inhibition. **H,** Orthogonal validation of proteins associated PI3K/Akt/mTOR signaling and the antioxidant response element (ARE) axis were assessed in DIPG cell lines following ONC201 exposure.

Figure 4. ONC201 in combination with paxalisib is synergistic across DIPG models. A, SU-DIPG-VI was treated with 5 μM ONC201 for 48 h, 20 mM NAC for 24 h and 1 mM H_2O_2 for 1 h, and protein changes downstream PI3K/Akt and reductase signaling were validated by Western blot. **B,** Western blot analysis of PI3K/Akt, Erk and antioxidant response element (ARE) signaling in SU-DIPG-XVII treated with 5 μM ONC201 (48 h) and 1 μM paxalisib (24 h). **C,** SU-DIPG-VI was grown in soft agarose in colony formation for 2 weeks treated with 0.5 μM ONC201, 100 nM paxalisib and the combination. The number of colonies were then quantified using ImageJ. Assay was performed in biological triplicate with representative images shown (One-way ANOVA, *$p<0.05$, **$p<0.01$ ***$p<0.001$ and ****$p<0.0001$, values shown as mean +/- SEM). **D-E,** DIPG cells SU-DIPG-VI, SU-

DIPG-XIII, SU-DIPG-XVII, were passaged, grown in low oxygen (5% O_2, 5% CO_2) or atmospheric oxygen (20% O_2, 5% CO_2) conditions for a week and then proliferation assays were performed using ONC201, paxalisib or both for 96 h (n=3). Synergy was determined using **D,** Chou-Talalay via CompuSyn or **E,** Bliss synergy analysis where a combination index (CI) where <1 (dotted line) demonstrates a synergistic effect and Bliss score >10 represents a strong synergism. **F-H,** Parental wt-*TP53* HSJD-DIPG-007 and HSJD-DIPG-007 cell lines transduced with a non-targeting control (NTC) gRNA, harboring knockout (KO) or knockdown (KD) of *TP53* were subjected to analysis following ONC201 treatment alone or in combination with paxalisib. **F,** Western blot confirmation of mitochondrial marker, SDHA, PI3K/Akt, Erk and ARE signaling to ONC201 (5 μM, 48 h). **G-H,** Cells were treated with increasing concentrations of ONC201, paxalisib or both for 96 h, in biological triplicate. Synergy was determined using **G,** Chou-Talalay or **H,** Bliss synergy analysis. Chou-Talalay and Bliss synergy graphs are reported as mean +/- SD.

Figure 5. ONC201 in combination with paxalisib is a synergistic drug combination in DIPG xenograft models. A, SU-DIPG-VI/Luc and HSJD-DIPG-007 cells were injected into the brainstem of NOD SCID Gamma (NSG) mice. Treatment was started at 4 or 3 weeks, respectively from xenograft date. ONC201 and paxalisib were administered by oral gavage. Xenografts were sacrificed for pharmacodynamics and survival was tracked where they were culled at ethical endpoints. **B-C,** Survival curve analysis of days post treatment start at animal sacrifice, with significance determined by survival curve comparison for **B,** SU-DIPG-VI and **C,** HSJD-DIPG-007. Shading indicates treatment duration. Log-rank (Mantel Cox) Test, *p<0.05, **p<0.01, ***p<0.001, ****p<0.0001. **D,** Tumor tissue from SU-DIPG-VI xenografts sacrificed at 2 weeks following start of treatment analyzed by Western Blot. **E,** SU-DIPG-VI *in vitro* cells exposed to 5 μM ONC201 0, 24, 48 and 72 hr compared to *in vivo* SU-DIPG-VI tissue collected from the prefrontal cortex (PFC) and brainstem (BS), treated with ONC201.**E,** Tumor tissue was resected from HSJD-DIPG-007 xenografts following 4 weeks of treatment and analyzed by immunohistochemistry. **F,** Sections were stained for H3K27M, Ki67 and SDHA (representative images are presented, scale bars = 2 mm, 200 μM or 50 μM). **G,** IHC images quantified via ImageJ (measured in technical triplicate, across biological replicates, n=3).

Figure 6. ONC201 in combination with paxalisib drives tumor regression and increased survival in DIPG case studies. A, Six-year-old *H3.1K27M, PIK3R1, ACVR1* mutant DIPG patient underwent biopsy soon after diagnosis and received 54 Gy radiotherapy over 30 fractions. MRI was performed six weeks after the completion of radiotherapy, and compassionate access was granted for the use of paxalisib to target *PIK3R1* mutations. Family of the patient sourced German ONC201 and started concurrently with paxalisib. **B,** Tumor size at diagnosis, following radiotherapy and throughout treatment. **C,** T2 and T1 post contrast MR axial scans at patient diagnosis, tumor area = 1554 mm^2. **D,** Following radiotherapy, tumor area decreased by 38.1% to 962 mm^2 compared to

diagnosis. **E,** MRI showed tumor area was stable following radiotherapy = 1156 mm^2, 20.2% progression. Following this scan, the ONC201 (15 mg/kg QW) and paxalisib (27 mg/m^2 daily) combination was started. **F,** MRI following 8 weeks on the combination tumor area was stable = 1224 mm^2, 6% increase. **G,** Tumor regression was seen after 20 weeks on the drug combination. Tumor area = 464 mm^2, tumor reduction by 62% compared to the last scan. **H,** Most recent MRI, tumor area = 306 mm^2, total tumor area reduction compared to diagnosis = 80%. **I,** The patient continues to remain on the combination 22 months following diagnosis. **J-P,** Sixteen-year-old *H3.3K27M, TP53, PIK3CA,* mutant DIPG patient received 54 Gy over 30 fractions. Patient enrolled on the ONC201 monotherapy trial NCT03416530 and experienced stable disease for 2 months. Following radiological and clinical progression, the patient received panobinostat (45 mg daily three times a week) with ONC201 (625 mg, once a week). Further progression was seen in the subsequent MRI, where the patient then received reirradiation. The patient immediately commenced ONC201 and paxalisib, both on compassionate grounds. **K,** Tumor area measured throughout treatment. **L,** T2 and T1 post-contrast MR axial scans at patient diagnosis, tumor area = 977.8 mm^2. **M.** MRI following first progression tumor area = 1303.3 mm^2. **N,** Patient received panobinostat in combination with ONC201, MRI image following the combination tumor area = 1814 mm^2. Following, this patient received reirradiation and ONC201 (15 mg/kg QW) and paxalisib (27 mg/m^2 daily) **O,** Tumor regression was seen 8 weeks post re-RT, whilst receiving ONC201 in combination with paxalisib, tumor area = 1322.6 mm^2. **P,** Tumor regression was again seen after 20 weeks on the combination, tumor area = 1209 mm^2, 20 months post diagnosis. Patient continued to receive ONC201 and paxalisib for the next 3 months and then contracted pneumonia and passed away 24 months from diagnosis.

Figure 1:

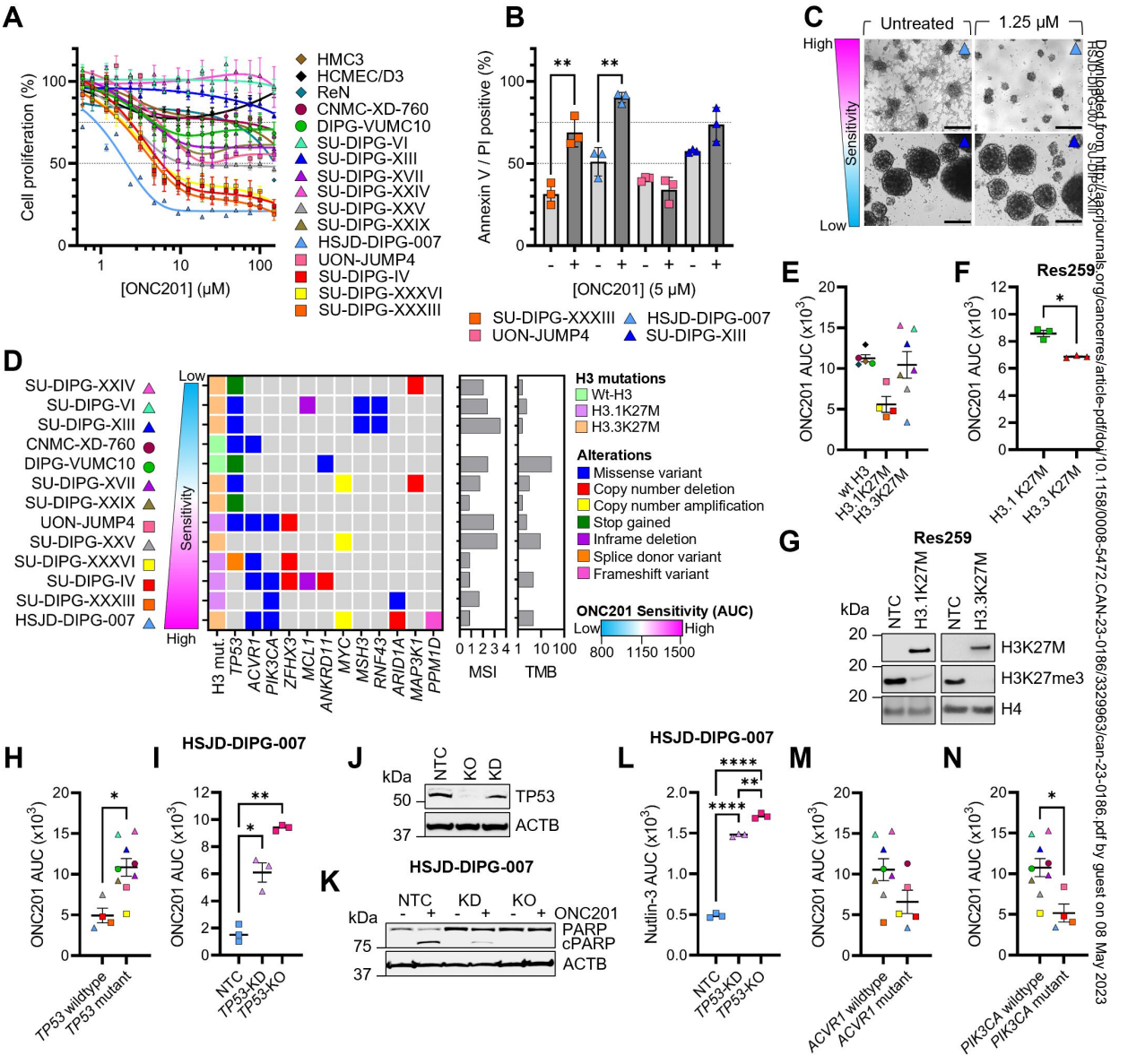

Figure 2:

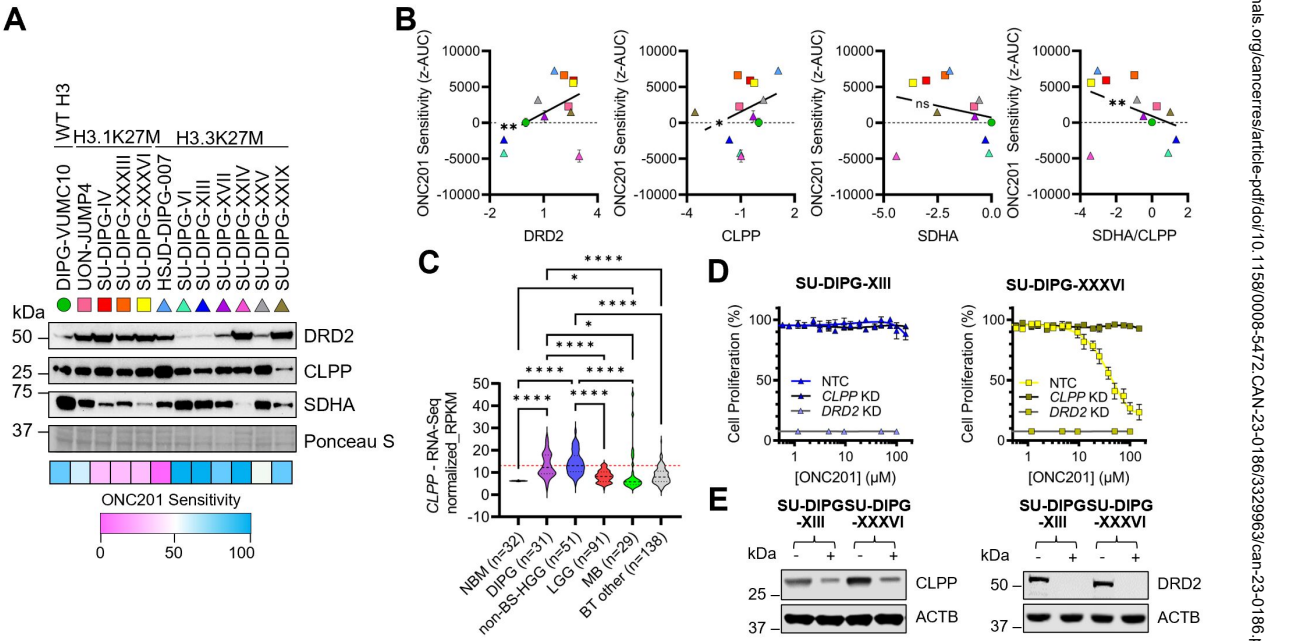

Figure 3:

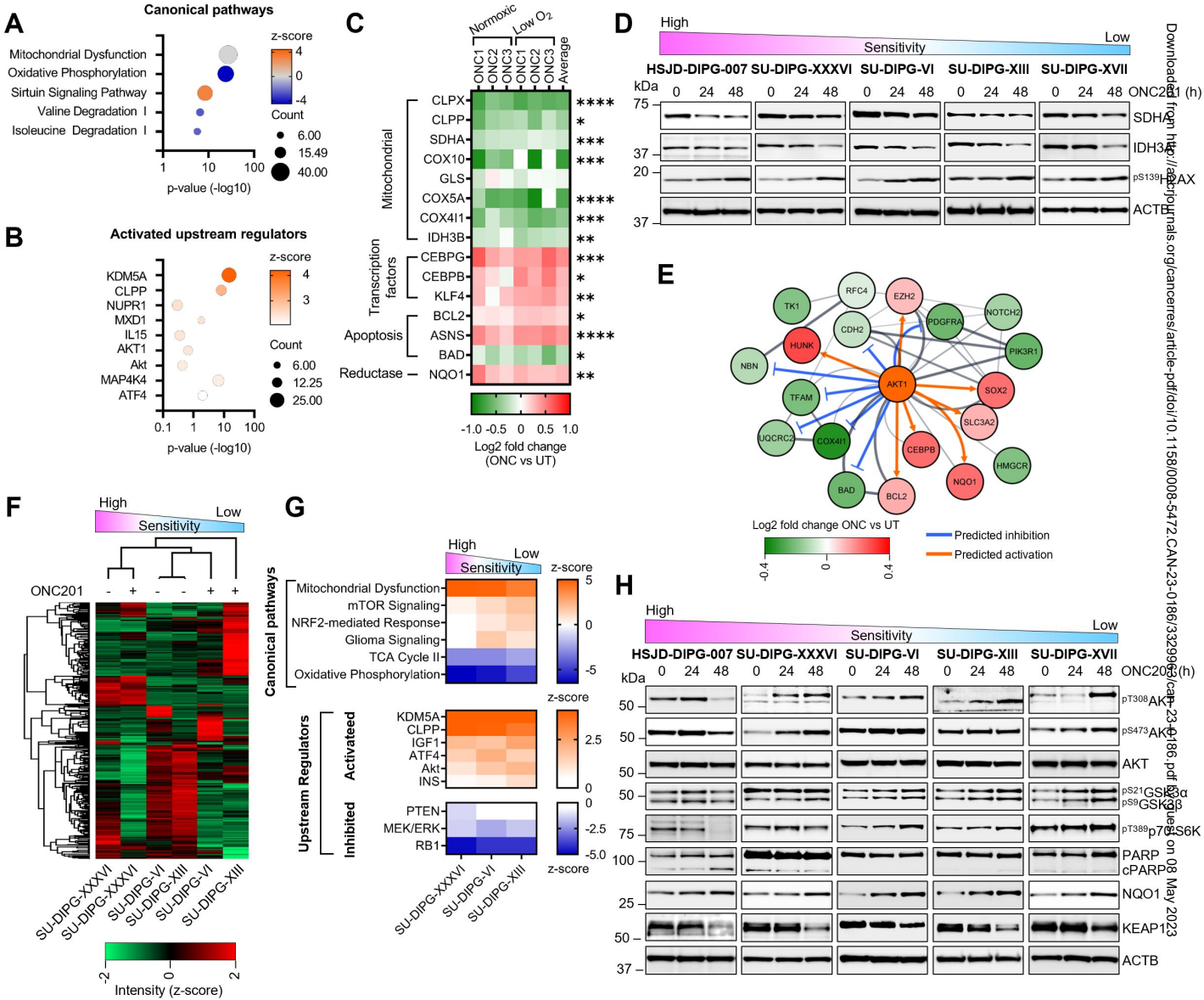

Figure 4:

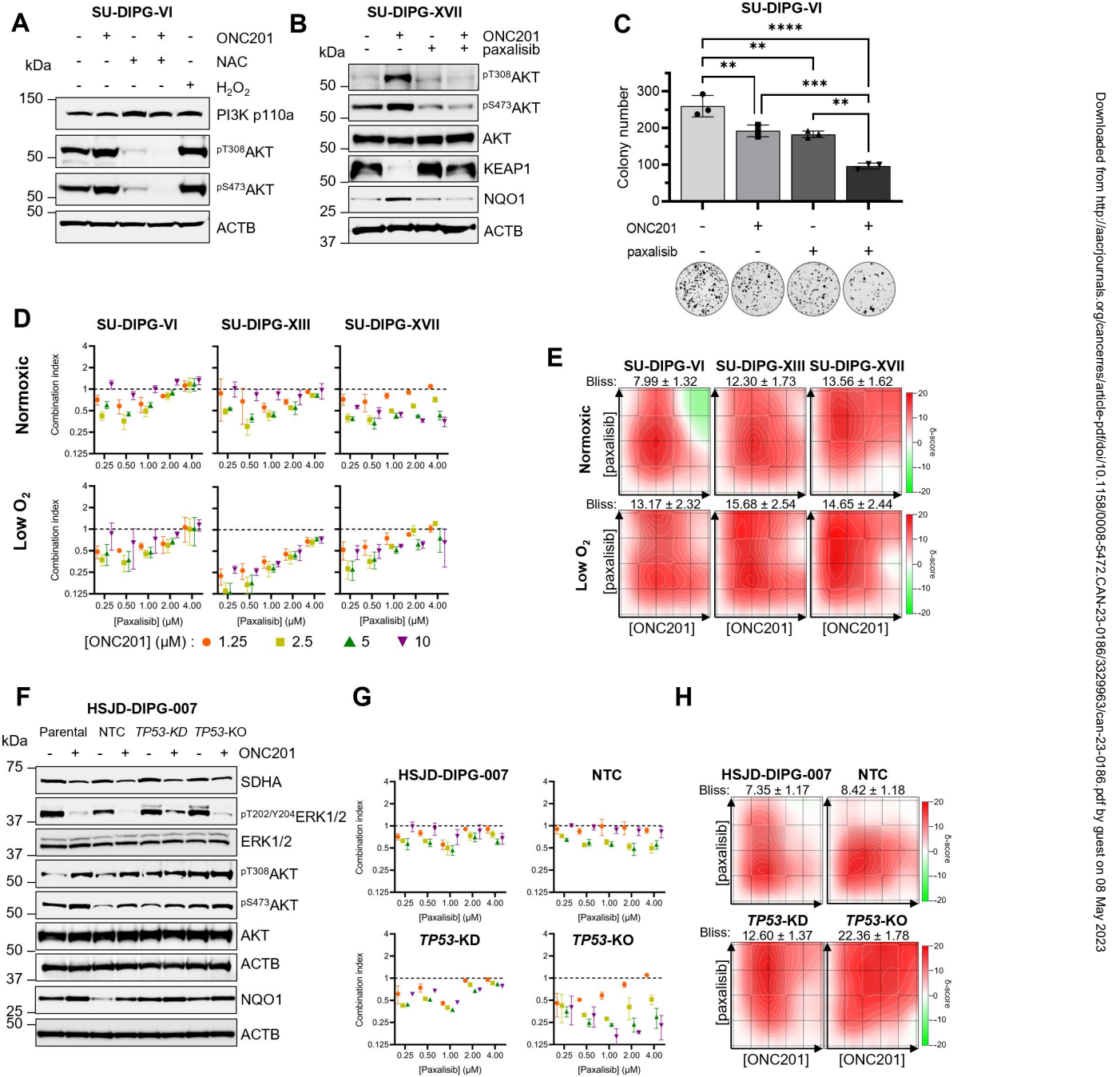

Figure 5:

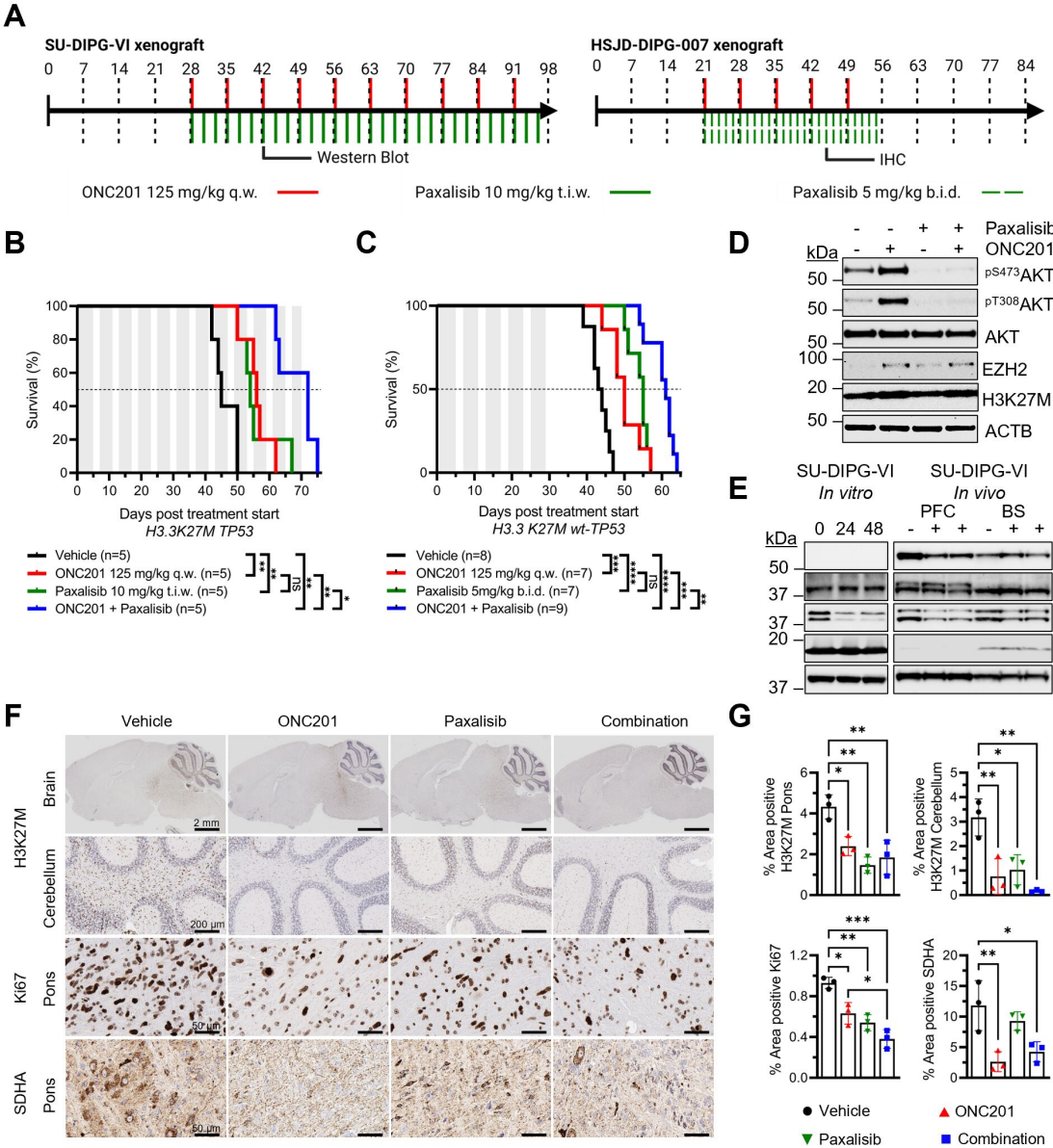

Figure 6: